Studying local earthquakes in the area Baltic-Bothnia Megashear using the data of the POLENET/LAPNET temporary array

O.A.Usoltseva[1] and E.G.Kozlovskaya[2,3]

[1] {Institute of Geospheres Dynamics of the Russian Academy of Sciences, Leninsky Prospect, 38, building 1, 119334, Moscow, Russia}

[2] {Oulu Mining School, University of Oulu, P.O. Box 3000, 90014 Oulu, Finland}

[3] {Sodankylä Geophysical Observatory, University of Oulu, P.O. Box 3000, 90014 Oulu, Finland}

Correspondence to: O.A.Usoltseva (kriukova@mail.ru)

Abstract

Earthquakes within areas inside continental plates are still not completely understood and the progress in understanding intraplate seismicity is slow due to short history of instrumental seismology and sparse regional seismic networks in seismically non-active areas. However, knowledge about position and depth of seismogenic structures in such areas is necessary, in order to estimate seismic hazard for such critical facilities as nuclear power plants and nuclear waste deposits. In the present paper we address the problem of seismicity in the intraplate area of northern Fennoscandia using the information on local events recorded by the POLENET/LAPNET temporary seismic array during the International Polar Year 2007-2009. We relocate the seismic events by the program HYPOELLIPS and grid search method. We use the first arrivals of P-waves of local events in order to calculate a 3-D tomographic P-wave velocity model of the uppermost crust (down to 20 km) for

selected region inside the study area and show that the velocity heterogeneities in the upper crust correlate well with known tectonic units. We compare position of the velocity heterogeneities with the seismogenic structures delineated by epicentres of relocated events and demonstrate that these structures generally do not correlate with the crustal units formed as a result of crustal evolution in Archean and Paleoproterozoic. On the contrary, they correlate well with the post-glacial faults located in the area of the Baltic-Bothnia Megashear (BBMS). Hypocentres of local events have depths down to 30 km. We also obtain focal mechanism of selected event with good data quality. The focal mechanism is of oblique type with strike-slip prevailing. Our results demonstrate that Baltic-Bothnia Megashear is an important large-scale, reactivated tectonic structure that has to be taken into account in estimating seismic hazard in northern Fennoscandia.

1 Introduction

The northern Fennoscandia has always been considered as an area of intraplate seismicity, with moderate-to-low seismic activity. Due to this, the story of instrumental seismology in the area is short and the present-day network of permanent seismic stations in the region is still not dense enough. That is why the progress on understanding where and when the earthquakes in the region may occur has been slow. Such areas are often considered as potentially attractive for such critical facilities as nuclear power plants, nuclear waste deposits and underground mines, for which proper seismic hazard estimates are required. Hence studying of local seismicity in intraplate areas benefits from deployment of dense temporary networks, like SVEKALAPKO (Bruneton et al., 2004; Hjelt et al., 2006; Sandoval et al., 2003; Sandoval et al., 2004). A new opportunity for investigating of intraplate seismicity in Fennoscandia was provided by the POLENET/LAPNET project.

POLENET/LAPNET was a sub-project of the multidisciplinary POLENET consortium (http://www.oulu.fi/sgo-oty/lapnet) related to seismic studies in the Arctic during the International Polar Year 2007–2009. The POLENET/LAPNET temporary seismic array was deployed in northern Fennoscandia (Finland, Sweden, Norway, and Russia). The array consisted of 35 temporary and 21 permanent seismic stations (Fig.1a). Most of the stations of the array were equipped with broadband three-component sensors. The array registered waveforms of

teleseismic, regional and local events from May 2007 to September 2009. The POLENET/LAPNET project became possible due to close cooperation of 12 organizations from 9 countries (see the list of organizations in Acknowledgements).

The northern part of the Fennoscandian shield is a region where the main part of the Earth crust was formed during Precambrian (Fig. 1b). The Paleoproterozoic (2.5-1.6 Ga) is the most important crust-forming period there. The Paleoproterozoic evolution of the shield can be divided into several major rifting and orogenic stages. The earlier Proterozoic events in the northern Fennoscandian shield are rifting of the Archean crust between 2.5 and 2.1 Ga, and consequent drifting and separation of the cratonic components by newly formed oceans (Lahtinen et al., 2008). During the later Paleoproterozoic, 1.95 – 1.8 Ga, the fragments of previously dispersed Archaean crust were partly reassembled, which resulted in formation of the collisional orogen. The region of our study (Fig. 1, Region 1) comprises non-reworked part of the Archean Karelian craton and the part reworked in the Proterozoic (Daly et al., 2006). The area is cut by ancient shear zones (Berthelsen and Marker, 1986; Talbot, 2001) and numerous faults, stretching both from NE to SW, from NW to SE and from N to S.

According to previous studies (Wu et al., 1999; Arvidsson, 1996, Slunga, 1991, Bungum et al., 2010, Redfield, Osmundssen, 2013, Redfield, Osmundssen, 2015), the local seismicity in northern Fennoscandia can be explained by two factors: a post-glacial rebound and spreading in the Mid Atlantic Ridge (Hess, 1962). According to Lidberg. (2010), the maximum vertical velocities in the post-glacial uplift area are observed at 19.5^0E/63.6^0N. In our study region the vertical uplift rate is varies from 7.7 mm/y to 9.9 mm/y. The post-glacial faults in Fennoscandia are relatively recent faults formed after the last deglaciation. They are usually several dozen kilometres long with large fault displacements (Kuivamäki et al., 1998, Lagerbäck and Sundh, 2008, Olesen et al., 2004).

The structure of the crust and upper mantle of the Fennoscandian shield is very complex. It has been studied by different active and passive seismic experiments (Guggisberg, 1986; Guggisberg et al., 1991; Hauser and Stangl, 1990; Sharov 1993; Luosto et al., 1989; Walther and Fluh, 1993; Kukkonen et al., 2006, Olsson et al., 2008, Eken et al., 2007). Detailed 2D P velocity models of upper crust along profiles in northern Fennoscandia were calculated in Silvennoinen et al. (2010) and Janik et al. (2009). Regional-scale 3D P-wave velocity model of the crust for our region was calculated in Glaznev (2003), Pavlenkova (2006).

Detailed investigation of the Pärvie fault, the world's longest known endglacial fault in the northern Fennoscandia, was performed in (Lindblom et al., 2015) on the base of data from permanent stations of the Swedish National Seismic Network and temporary network (2007-2010 y) around the Pärvie fault. Authors used the waveform cross-correlation technique for detection of microearthquakes near the Pärvie fault and HypoDD program to improve the location. They found the remarkable correlation between the seismicity and the mapped endglacial fault scarps. They obtained new 1D velocity model for this region. The deepest earthquakes were fixed near the depth 35 km by them. Authors estimated that the endglacial Pärvie earthquake had a magnitude of 8.0 ± 0.4.

The data of the POLENET/LAPNET array was used in several studies aiming to obtain seismic velocity structure of the crust and upper mantle in northern Fennoscandia. A 3D S-wave velocity model of the upper crust was obtained by ambient noise tomography (Poli et al., 2013). In Silvennoinen et al. (2014) the new map of the crust–mantle boundary was obtained for the POLENET/LAPNET study area using both previous controlled-source seismic profiles and P-wave receiver functions estimated for POLENET/LAPNET stations. Teleseismic P-wave velocity model of the upper mantle beneath northern Fennoscandia was obtained by Silvennoinen et al. (2015) using teleseismic travel time tomography. The evidence of upper mantle seismic anisotropy was presented by Plomerova et al. (2011) and Vinnik et al.(2014).

The aim of the present paper is to obtain accurate coordinates of hypocentres of local events recorded by the POLENET/LAPNET array, delineate position and depth penetration of seismogenic structures and to obtain focal mechanisms of selected earthquake. In our study we relocate 34 local earthquakes. Another purpose of our study is to use the local events data (36 earthquakes and 9 explosions) in order to calculate a 3-D tomographic model of the uppermost crust (down to 20 km) for selected region inside the POLENET/LAPNET study area and to obtain new information about structure of the crust there. The present work is continuation of the previous study Usoltseva et al. (2012).

2 Data and velocity model

The seismic stations of the POLENET/LAPNET array were installed in quiet sites. The average spacing between stations is equal to 70 km. The stations recorded continuous data with sampling rate varying from 50 to 100 sps. Waveforms were stored in the standard seismological

miniSeed format (http://www.iris.edu/manuals/SEEDManual_V2.4.pdf) in RESIF data centre hosted at University Joseph Fourier (http://portal.resif.fr).

Initial information about origin time and hypocentre coordinates of local seismic events was obtained from the seismic catalogue from all the Nordic countries, hereafter FENCAT catalogue (www.seismo.helsinki.fi). According to the FENCAT catalogue, 9174 explosions and 234 earthquakes in northern part of Fennoscandian Shield occurred during the POLENET/LAPNET data acquisition period. The majority of explosions originated from known quarries, including clusters of epicentres around Kittila gold mine (~200 events), Kiruna mine (~3000 events), Malmberget mine (~4000 events), and the Kovdor and Zapoliarni areas in Russia (~400 events in both areas). In our study we used a set of local earthquakes and explosions with more than 6 first arrivals of P-waves recorded by the POLENET/LAPNET array. Epicentres of these events are shown in Fig. 2. The seismic waveforms were reviewed with the Seismic Handler (SHM) program package (Stammler, 1993, http://www.seismic-handler.org/portal). Recordings were band-pass filtered with corner frequencies at 1 and 15 Hz and amplitude-normalized. Examples of seismograms (Z component) of two local events with different focal depth and one local explosion are shown in Fig. 3 (a,b,c).

As can be seen, arrivals of P-waves are present at offsets of 25-232 km. Shallow local earthquake with magnitude ML 2.2 and deep earthquake with magnitude ML 1.6 have distinct P- and S-wave arrivals, particularly at the short offsets (Fig. 3a and Fig. 3b). The local explosion (Fig. 3c) with ML=1.1 has less distinct first arrival of S-wave, that is explained by complex source mechanism as explosions are usually done in series. For deep earthquake we observe strong S-wave arrivals and weak P-wave arrivals at distances less than 100 km from the epicentre. These amplitudes are also influenced by the radiation pattern of the earthquake. The same tendency for amplitudes of the first arrivals of P- and S-waves was noticed by (Arvidsson et al., 1992) for Skovde earthquake with ML of 4.5. The strongest earthquake took place on 19.01.2008 at 19:52 (67.23^0N 23.80^0E, dep=10.4 km, ML=2.2, HEL).

As shown by Majdanski et al. (2007), the reliable recognition of different phases of body waves propagating through a 3D structure and picking of their arrivals requires calculation of theoretical travel times using some a-priori known velocity model.

In our study we used the 1D velocity model of the HUKKA-S profile (Fig. 1b) published by Janik et al. (2009). The original model consists of 6 layers in the crust and 2 layers in upper mantle. In our work we use a simplified version of this model (Table 1) with 5 crust layers and 2 mantle layers. Two upper layers were replaced by one single layer because of their small thickness (0.5 and 0.8 km, respectively). At initial stage the trajectories of direct and refracted seismic rays were calculated using the Snell's law.

Propagation of P-wave rays through the velocity model (Table 1) is shown in Fig. 4 and Fig. 5 for shallow and deep earthquakes, respectively, at offsets of 20-250 km. Minimal travel time corresponds to direct rays for a shallow earthquake at offsets less than 200 km with the take-off angles less than 90 degrees. For a deep earthquake the first arrivals of P-waves correspond to the direct waves at short distances and the waves refracted at the Moho boundary at long distances. Therefore the travel times of the first arrivals depend on the velocity structure of the upper crust for shallow earthquakes and of the whole crust and upper mantle for deep earthquakes. This is important both for focal mechanisms evaluation and for local events tomography.

For shallow earthquakes the confusion between different seismic phases (direct wave and the wave refracted at the C2 boundary, see Fig. 4) can occur at offsets of 50-100 km. For events with hypocentre depths of more than 20 km the waves refracted at the C1 and C2 boundaries are absent. For such events the confusion between different seismic phases may occur at offsets more than 170 km. Thus the erroneous determination of the first P-wave arrival is more probable for shallow earthquakes. In order to avoid such confusion we calculated theoretical travel times of direct and refracted P waves for each event and stations using the model from Table 1. After comparison of observed and calculated reduced travel times graphically (examples of such comparison are presented in upper plots of Fig. 4 and Fig. 5) and detecting the erroneous phase determinations we compiled a dataset of arrival times for each station (Fig. 1a) and for each event (Fig. 2). The arrival times were picked at seismograms of stations with distances less than 250 km from the epicentre.

4 Relocation of events

For location of events we used two different methods. One of them is HYPOELLIPS (Lahr, 1989). This is an iteration method for minimization of the root-mean-square residuals (RMS) between observed and calculated travel times using solution of underdetermined system of linear equations. In HYPOELLIPS the residuals are weighted as a function of distance, azimuth and depend on data quality. Damping is used in order to ensure convergence. In each iteration the damping is changed depending on the RMS value. For error estimation a 68% joint spatial confidence ellipsoid is calculated for each hypocentre (Lahr, 1989). The sizes of this ellipsoid are defined by the estimated standard error of arrival times (SD) and the weight code (W) assigned to each arrival time. In our study we used SD≤0.07 s for W=0, SD≤0.35 s for W=1, SD≤0.7 s for W=2. The epicentral and depth statistical uncertainties at the 68 % confidence level were evaluated from the correspondent ellipsoids and are presented in Table 2 and Table 3. In practice the uncertainty in hypocentre determination due to using different methods, different data and different velocity models is larger than statistical uncertainties.

The other method is a grid search method (Nelson and Vidale, 1990), in which global minimization of the RMS difference between observed and calculated travel times is performed. In our study we used our own programming realization of the method. This grid search method is uniform for arbitrary complex velocity models and has the same computation time for 1D and 3D velocity models. Originally, minimization was performed using objective functions both in L_1 and L_2 norms. But for the final relocation we selected the L_2 norm because the L_2 norm provided more precise hypocentre coordinates during testing of inversion algorithms with the data of local explosions with known coordinates. The study area was gridded with 500 by 500 by 60 grid points (1 km spacing). The transformation between the spherical coordinate system of the Earth to the Cartesian grid was performed by short distance conversion. The method utilizes finite difference computation of the first arrival times (Podvin and Lecomte, 1991). In contrast to HYPOELLIPS, the residuals of travel times are used without weighting. The lower limit of the error in hypocentre determination is equal to the step of the grid (1 km). In our study we used the grid search method also for investigating stability of solution.The above described relocation methods were tested using local explosions from the Hukkavaara hill, for which coordinates of hypocentres are known with high precision (master events) and arrival times of the first arrivals of P and S waves. Example of the Hukkavaara explosion with ML=1.5 is presented in Fig. 6, in which event waveforms recorded by the temporary

141 station LP53 and the permanent station HEF are shown. The distance between the explosion and the stations is equal to 59 km for LP53 and to
142 103 km for HEF. In seismograms we can see an acoustic signal that is one of the explosion indicators. In station LP53 the maximal amplitude
143 of the acoustic signal is considerable larger than the maximal amplitude of the seismic signal. At offset of 103 km this amplitudes have similar
144 values. Thus in our case the acoustic signal attenuates faster than the seismic one. This is explained by strong dependence of acoustic wave
145 propagaion on weather conditions.

146 The results of testing are presented in Table 2. We found out that the difference of event coordinates obtained by both methods for different
147 explosions is less than 3.7 km, while the difference in origin times is less than 0.1 seconds. The RMS is less than 0.3 second for both methods
148 and hypocentre depths are close to zero. Table 2 presents the results for gap values of 47^0 and 117^0, and for epicentre distances of 24-267 km,
149 25-179 km, and 59-239 km, respectively.

150 Table 3 presents results of relocation of 34 events from Region 2 by both methods using the first arrivals of both P and S waves. After
151 relocation we obtained the RMS error that less than 0.4 s for 85% of events. The importance of relocation with the help of temporary stations
152 follows from the analysis of hypocentre information from the FENCAT catalogue. As seen from Table 3, the hypocentre depth of eight events
153 was not determined precisely, but fixed in FENCAT. In addition, 20 events from 34 have the nearest station that is the temporary station of the
154 POLENET/LAPNET array. The number of observations at temporary stations prevails upon the observations at permanent station for 22
155 events.

156 We performed relocation with the first P wave arrival times only and also with both first P and S wave arrivals. The difference between
157 coordinates obtained using P waves and using both P and S waves is less than 7 km. The hypocentre depths obtained using P waves and using
158 both P and S waves are identical, but for some events (for example the event 23.10.2008 at 18:41 UTC) the depth difference is equal to 11 km.
159 We noticed that location using only P waves is more sensitive to the weight coefficients in the HYPOELLIPSE. Thus the results of relocation
160 using P and S waves are more similar for calculations using two different methods (HYPOELLIPSE and grid search).

Events from Table 3 were divided into four groups. The first group contains 2 events, for which the location was not stable. We assume that location is not stable if the difference between hypocentres depths obtained by two methods is more than 8 km or the error for the hypocentre depth obtained by the HYPOELLIPSE is more than 8 km. For the second group of 23 events we obtained stable hypocentre solutions and depths less than 20 km. The third group consists of 2 events with hypocentres near the surface. Hypocentres of the forth group of 7 events have stable solutions and depth of more than 20 km.

The comparison of hypocentre coordinates with those from the FENCAT catalogue showed that the latitude differences are less 7 km, while the longitude differences may reach values of 8-12 km. The hypocentres of most of the natural events from Table 3 are deeper than the hypocentres presented in FENCAT catalogue. This difference can be explained by different velocity models used for events location, larger number of observations, stations distribution and higher density of stations, In Table 3 the stars denote the events with one and more stations satisfying the condition $\Delta<2*h$, where Δ is an epicentral distance and h is the hypocentre depth. For these events we expect more reliable determination of depth. For investigating the stability of the depth determination we analyzed the depth RMS error using the grid search method. The local minimum of RMS in the depths is presented in Table 3

For groups of shallow earthquakes the precision of depth determination is lower than that for the group of deep events. It can be explained by higher probability of erroneous phase determination for surface events at large distances from the epicentre. The comparison of the observed and theoretical travel times before and after relocation is shown in Fig. 7 for one selected shallow earthquake. The correspondent seismograms are presented in Fig. 3a. The small difference between new and old residuals suggests that the quality of hypocentres in the FENCAT catalogue is satisfactory for the similar events from this region.

The earthquakes from the group of deep events are also indicated as the deep ones in the FENCAT catalogue with the exception of event on 09.03.2012 at 22:42 UTC. After relocation the possible depth of them varies from 21 to 53 km. For deep events we can see that differences in hypocentre depths and coordinates determined by both methods are less than 3.3 km. The azimuthal gap varies from 61 to 122 degrees. The hypocentres of deep earthquakes are located in an elongated N-S oriented area (Fig.2 and Fig.18). The comparison of calculated and observed

travel times before and after relocation is presented in Fig. 8 for the event with the initial hypocentre depth of 12 km and the final one of 30 km. After relocation the RMS became 0.38 s for HYPOELLIPS and 0.34 for grid search method. Figure 9 (a,b) shows comparison of travel times of P- and S- waves observed at stations of the LAPNET array with theoretical travel time of direct P- and S waves for event on 07.06.09 on 02:52 UTC with ML=1.7 and depth of 53 km. This is the deepest earthquake from all events considered in our study. We observe large scatter in first arrivals of P and S waves. The mistake connected with erroneous determining of arrival times can be excluded because of very sharp impulsive arrivals (Fig. 9c). The possible explanation of the scatter is the difference in seismic velocities beneath different groups of stations that is not possible to take into account in 1D model used for relocation. The absence of auxiliary P phases between the first arrivals of P and S waves may indicate absence of the boundary below the hypocenter and hence large source depth. This earthquake is situated near the end of the system of Palojärvi, Paatsikkajoki and Kultima faults. Analysis of seismicity map from [Korja, Kosonen, 2015] shows that one deep earthquake was recorded earlier along the same postglacial fault branch.

5 Focal mechanisms of selected events

For determination of focal mechanisms we used the program HASH (Hardebeck and Shearer, 2008), that estimates earthquake focal mechanisms from the first-motion polarities. We assumed that the earthquake source can be considered as a point source with a double-couple mechanism and that the rupture dimension in the source is much smaller than the distance to the stations and the wave length considered. The velocity model presented in Table 1 was used to determine take-off angles. The program HASH performs grid search over all possible values of strike, dip and rake angles. The polarity of signals at all stations was tested using strong teleseismic events. For visualization of focal mechanism solutions we used the software from “Computer programs in seismology” (Herrmann and Ammon, 2002) and Matlab script bb.m written by Andy Michael, Chen Ji and Oliver Boyd.

P wave first-motions were determined for events on 19.01.2008 at 19:52 UTC, 13.09.2008 at 07:21 UTC, 09.11.2008 at 17:00 UTC, 22.09.2008 at 14:30 UTC. We selected the event on 13.09.2008 at 07:21 UTC for detailed analysis because of the minimal fault plane

uncertainties and the high quality class. This earthquake is the shallow event with ML=1.9 (Fig. 2). For the computation we used parameters of hypocentres determined by grid search method (Table 3). Results of focal mechanism calculations are presented in Table 4.

The data used consists of 22 first motion polarities. Signals corresponding to compressions are observed at 9 stations, from which 8 are impulsive and 1 is emergent. Signals corresponding to dilatations are observed at 13 stations, from which 11 are impulsive and 2 is emergent. The seismograms for the event showing the first motions are presented in Fig. 10. In Fig. 11 one can see lower hemisphere equal area projections of the focal sphere for researching events and P wave first-motion data in focal sphere. Four points are inconsistent with the given deformation model but they are presented for correct statistical evaluation. We observe good azimuthal coverage and the range of take-off angles of 68^0-128^0. For demonstration of uncertainty range the set of 150 acceptable mechanisms and the distributions of acceptable dip, rake and strike for these solutions are shown in Fig.11

The stability of a focal mechanism with respect to polarity errors was tested by a bootstrap procedure, that is, by removing a single polarity data points consequently and observing the change in the best-fitting mechanism. The stability with respect to different velocity models was controlled by using velocity models from different studies (Silvennoinen et al., 2010, Janik et al., 2009, Silvennoinen et al., 2014). The tests confirmed the stability of solution. The optimal result was received with the velocity model for station HEF (Silvennoinen et al., 2014). As follows from the dip value, the hanging wall dip is close to the 60^0-90^0. As follows from the strike, the direction of the fault plane is deviated by 0^0-20^0 from the N-S direction clockwise or the direction is NWW-SEE. The focal mechanism is of oblique type with strike-slip prevailing.

6 Local events tomography

Local event tomography was used for estimating the P-wave velocity structure in the upper crust of our study region. The procedure consists of two steps. The first one is improvement of the a-priory 1D model (Table 1), calculating station corrections and relocating the events in the new 1D model using the program VELEST (Kissling, 1988; Kissling et al. 1994) and the known hypocentre parameters. The second part

223 incorporates consecutive inversion for the 3D velocity model and hypocentres coordinates using the SIMULSPS14 program (Thurber, 1983;
224 Eberhart-Phillips, 1993; Thurber, 1993). In this code the raytracing is performed by shooting method of Virieux et al. (1988), where the ray
225 connecting station and receiver in the given velocity model is found by varying the initial azimuth and take-off angle at the source. The 3D
226 velocity model is parameterized by regular grid and the velocity model is described by linear B splines. The velocity inversion is performed
227 by damped least-squares method and resolution matrix is estimated simultaneously. The calculations were performed both with synthetic and
228 real data.

229 As a starting model, we used the velocity model from Table 1. VELEST run with a total of 36*4+9+50+2=205 unknowns and 624 rays: 311
230 direct and 313 refracted. The over-determination factor of the inverse problem is approximately 3. The maximum number of hypocentres (25)
231 is located between 1.3 and 18 km. The number of observations for each station varies from 1 to 37. The RMS residuals for all events are
232 decreased by 8% after the third iteration. The velocities were modified only in the layers between 1.3 and 18 km and between 18 and 37 km.
233 Final velocity values in these layers have changed less than 0.1 km/s compared to the initial values. After the third iteration the relocated
234 hypocentre parameters differed from the initial ones by less than 2.3 km in horizontal direction and less than 1.5 km in vertical direction.

235 According to (Kissling, 1988), the station corrections should reflect the basic features of surface geology. Only the corrections for stations
236 with many observations in different azimuth directions may be accounted for lateral variations in the shallow subsurface, however. The station
237 corrections used in inverse problem are shown separately in Fig.12 for the stations that registered more than 10 observations of the first arrival
238 of P-wave. The maximum number of arrivals was observed at the permanent station HEF. That is why it was selected as a reference station.
239 As seen from Fig. 12, the negative time corrections prevail in the northern part of the area, while in the South-East the positive time
240 corrections are observed. The corrections that are probably linked to the superficial geology were obtained, for example, for stations KTK1
241 (elevation 365 m, negative), LAN (elevation 500 m, negative), LP21 (elevation 94 m, positive), LP31 (elevation 139 m, positive). The
242 correction of NIK station is connected with the edge effects, because of the station NIK is situated near western boundary of the studied
243 region, has the elevation of 300 m and simultaneously the large positive correction.

SIMULPS14 was run with 36*4+9=153 hypocentre variables, 299 velocity adjustments and 621 times first P arrivals. The over-determination factor was 1.6. This is the low value, but it is enough for determination of large-scale velocity heterogeneities in our study area assumed that the ray coverage and resolution tests are in order. The ray coverage is presented in Fig.13. The high ray density is observed at the depths 0-20 km. In the present study the distance between adjacent grid nodes equals 70 km in x direction and 50 km in y direction.

The resolution was analysed through several checkerboard tests. The synthetic checkerboard velocity model was calculated by varying the velocity as a sinusoidal function in the x and y directions. The maximum amplitude of positive and negative velocity perturbations was 6% with respect to a background velocity model (Table1). Because of small amount of local events in our area and large-scale model grid it was necessary to evaluate the minimal size of heterogeneities that could be reconstructed. Therefore we perform synthetic tests with the cells of 75*75 km and 100*100 km (Fig. 14). We obtained bad reconstruction results for grid with 75*75 km cells and good results for grid with 100*100 km cells. This means that minimal reliable size of revealed velocity anomalies is about 100 km for our data. As the geological terrains in the study area (Fig. 1b) have generally elongated form, we performed the next resolution test with anomalies of 150*75 km (Fig. 15). The tests were performed to analyse the reconstruction picture with normal grid orientation and grid turned by 30^0. As can be seen, all heterogeneities are reconstructed nearly perfectly at depths down to 18 km in the central part of the model. Comparison of Fig.15a and Fig.15b shows that the shape of anomalies (especially of high velocity anomalies) depends on grid orientation. The true boundary of discontinuity is determined better when it coincides with the grid line (Fig 15).

Results of inversion with real data and with different grids are presented in Fig. 16, in which the horizontal cross-sections of the final velocity model are shown for 1.3 km, 10 km and 18 km depths. The deviations of P-wave velocities from the 1D background velocity model (Table 1) do not exceed ±5%. The RMS misfit decreased from 0.32 s to 0.27 s in normal grid (Fig.15a) and from 0.32 s to 0.25 s in rotated grid (Fig.15b). After relocation in SIMULPS14 the maximum vertical deviation of event hypocentres equals to 5 km and the maximum horizontal deviation equals to 3 km. From Fig. 16 one can see a high velocity zone in the northern part of the study area that continues to a depth of

about 10 km. High velocities are observed to the west of 24^0E, while low velocities prevail to the east of it. The elongated low velocity area stretching NE-SW is seen in the western part of region around 67^0N. This area becomes more visible with depth.

7 Discussion and conclusions

In spite of low seismic activity during the POLENET/LAPNET data acquisition period, it was possible to obtain accurate and reliable coordinates of hypocentres for a number of local earthquakes and to calculate one focal mechanism. We also reconstructed a 3-D P-wave velocity model of the upper crust to a depth of about 18 km for the area that has not been studied previously using seismic tomography techniques. Recently local seismic tomography research was performed for others areas in northern Fennoscandia (Lindblom et al., 2015). Lindblom et al. (2015) concentrated on the relocation and optimal average 1D model, while the 3D velocity model was not discussed in details. In the present study the 3D velocity structure is of the primary interest. Generally, our results provide new knowledge about the structures along which the intraplate seismicity in the northern part of the Fennoscandian shield is concentrated.

As seen from the Fig. 16, the P-wave velocity anomalies in the area with the good resolution are smaller than ±5 % with respect to the initial velocity model. The lateral heterogeneities in the upper crust in our velocity model are show general good correlation with the surface geology and are in agreement with the 3D S-wave velocity model obtained by Poli et al. (2013) by ambient noise tomography as well as with the 2D P- and S-wave velocity models along the POLAR profile (Janik et al., 2009) and P-wave velocity model along the southern segment FIRE4 profile (Silvennoinen et al., 2010). The high velocity anomaly correlates partly with the 2.1 Ga Greenstones area and partly with the Lapland Granulite Terrane (Fig. 1). These units correspond to the high P- and S-wave velocity zones in the upper crust in the model by Janik et al. (2009). Poli et al. (2013) also detected the high S-wave velocity anomaly corresponding to this unit.

The low velocity anomaly in the southern part of our study area is observed in the range of depths from 0 to 5 km and it disappears at a depth of 10 km (Fig. 16). This anomaly correlates with the southern part of the Lapland Granitoid complex (LGC) and Peräpohja Schist belt (Fig. 1).

The LGC is seen also as a low S-wave velocity anomaly in the model by Poli et al. (2013). Silvennoinen et al. (2010) calculated high-resolution P-wave tomographic velocity model and discovered a highly reflective high velocity and high density body beneath the LGC with the upper boundary at a depth of 1-3 km. This feature revealed by high-resolution seismic survey is not seen in our model that was parameterized with large blocks. The low velocity anomaly located approximately at the Finnish-Swedish border at a depth of 18 km does not correlate with any geological unit and might be an inversion artefact.

Comparison of velocity anomalies revealed by seismic tomography (Fig. 16) with position of hypocentres of earthquakes and post-glacial faults (Fig. 17) suggests that seismogenic structures in our study region do not correlate with the boundaries of geological units formed in Archean and during their subsequent reactivation in Proterozoic. However, they show good correlation with known post-glacial faults in the region, which agrees also with the results obtained by Lindblom et al. (2015). These post-glacial faults are generally located within a broad N–S-directed zone running from the Bothnian Bay to the Atlantic Ocean. This zone coincides with the old Precambrian Baltic-Bothnia Megashear zone (BBMS) (Berthelsen and Marker, 1986), interpreted in (Lahtinen et al., 2003) as an old plate boundary.

Van Lanen and Mooney (2007) proposed that such ancient suture zones have a high probability of reactivation. They also showed that existence of deeply penetrating crustal faults is the major parameter that controls distribution of intraplate earthquakes in stable continental region of North America. The deepest earthquakes in our study area are shown in Fig. 17 (FENCAT) and Fig. 18 (Table 3). They are located along the BBMS, although not all of them can be associated with known post-glacial faults. According to (Arvidsson, 1996) the deepest earthquakes from the Lansjärv fault and the Lainio-Suijavaara fault have focal depths of 34 and 37 km, respectively. In our research the seismic events at Lansjärv and Lainio-Suljavaara faults located in the BBMS area have the hypocentres depths up to 20 km. The deep earthquakes have been detected also on other post-glacial faults (Lindblom et al. 2015, Juhlin and Lund, 2011). Fig. 18 summarizes the available fault plane solutions for the earthquakes in the area of BBMS. The information about sources of these earthquakes is presented in Table 4 (our study) and Table 5 (previous studies). As seen, all the focal mechanisms with exception of Event 4 (Table 5) have a pronounced strike-slip faulting and shear movement component. This is in contrast with the conclusion made by (Arvidsson, 1996), who interpreted the

most of northern Fennoscandian postglacial earthquakes as signatures of progressive rapid rise of the land from the centre of post-glacial rebound (Nocque et al., 2005). Also the world stress map 2008 (http://dc-app3-14.gfz-potsdam.de/pub/stress_maps/stress_maps.html) shows 4 thrust faulting stress indicators in northern Fennoscandia, which are typical for the process of rebound.

Recently, Steffen et al. (2014) showed that depth of the fault tip and angle of the fault plays an important role in reactivation of faults by deglaciation processes. They find that steeply dipping faults (~75°) can be activated after glacial unloading if the assumed coefficient of friction in the rock is low, and fault activity continues thereafter. This agrees with the results of our study that shows that seismicity in the BBMS occurs at the steeply dipping faults penetrating to a depth down to 30 km. This also can be a possible explanation why this activity continues nowadays. It should be noted that the model events in the study by Steffen et al (2014) have the reverse faulting mechanisms, not strike-slip ones considered in our study.

Generally, our study shows that the BBMS is an important reactivated large-scale tectonic suture in northern Fennoscandian shield that extends to greater depths. This is necessary to take into account in estimating seismic hazard in the area.

Acknowledgements

The authors appreciate the efforts of organisations operating permanent seismograph networks of Finland (the Institute of Seismology of the University of Helsinki and Sodankylä Geophysical Observatory of the University of Oulu Oulu) and Swedish National Seismic Network in Uppsala, which contribute the data for the FENCAT catalogue. The POLENET/LAPNET project was a part of the International Polar Year 2007-2009. Equipment for the temporary deployment was provided by RESIF–SISMOB, FOSFORE, EOST-IPG Strasbourg Equipe seismologie (France), Seismic pool (MOBNET) of the Geophysical Institute of the Czech Academy of Sciences (Czech Republic), the Sodankylä Geophysical Observatory (Finland), the Institute of Geosphere Dynamics of RAS (Russia), the Institute of Geophysics ETH Zürich

(Switzerland), the Institute of Geodesy and Geophysics, the Vienna University of Technology (Austria), and the University of Leeds (UK). Funding agencies provided support for organisation of the experiment are: Finland : The Academy of Finland (grant No. 122762) and University of Oulu, France: BEGDY program of the Agence Nationale de la Recherche, Institute Paul Emil Victor and ILP (International Lithosphere Program) Task Force VIII, Czech Republic: grant No. IAA300120709 of the Grant Agency of the Czech Academy of Sciences. Russian Federation : Russian Academy of Sciences (programs No 5 and No 9).

The POLENET/LAPNET working group members are Elena Kozlovskaya, Helle Pedersen, Jaroslava Plomerová, Ulrich Achauer, Eduard Kissling, Irina Sanina, Teppo Jämsén, Hanna Silvennoinen, Catherine Pequegnat, Riitta Hurskainen, Robert Guiguet, Helmut Hausmann, Petr Jedlicka, Igor Aleshin, Ekaterina Bourova, Reynir Bodvarsson, Evald Brückl, Tuna Eken, Pekka Heikkinen, Gregory Houseman, Helge Johnsen, Elena Kremenetskaya, Kari Komminaho, Helena Munzarova, Roland Roberts, Bohuslav Ruzek, Hossein Shomali, Johannes Schweitzer, Artem Shaumyan, Ludek Vecsey and Sergei Volosov. We thank the anonymous reviewers for valuable comments that helped us to improve the manuscript.

References

Ahmadi, O., Juhlin, C., Ask, M., and Lund, B.: Revealing the deeper structure of the end-glacial Parvie fault system in northern Sweden by seismic reflection profiling, Solid Earth, 6, 621-632, www.solid-earth.net/6/621/2015/ doi:10.5194/se-6-621-2015, 2015.

Amante, C. and Eakins, B.W.: ETOPO1 1 Arc-Minute Global Relief Model: Procedures, Data Sources and Analysis, NOAA Technical Memorandum NESDIS NGDC-24, National Geophysical Data Center, NOAA, doi:10.7289/V5C8276M, 2009.

Arvidsson R.: Fennoscandian Earthquakes: Whole Crustal Rupturing Related to Postglacial Rebound, Science, 274, 5288, 744-746, doi: 10.1126/science.274.5288.744, 1996.

Arvidsson R., Wahlstrom R. and Kulhanek O.: Deep-crustal earthquakes in the southern Baltic Shield, Geophys. J. Int., 108, 767-777, 1992.

Berthelsen, A. and Marker, M.,: 1.9- 1.8 Ga old strike-slip megashears in the Baltic Shield, and their plate tectonic interpretation, Tectonophysics, 128, 163-181, 1986.

Bruneton, M., Pedersen, H.A., Farra R., Arndt N.T., Vacher P., Achauer U., Alinaghi A., Ansorge J., Bock, G., Friederich, W., Grad, M., Guterch, A., Heikkinen, P., Hjelt, S.E., Hyvonen, T.L., Ikonen J.P., Kissling, E., Komminaho, K., Korja A., Kozlovskaya, E., Nevsky, M.V., Paulssen, H., Pavlenkova, N.I., Plomerova J., Raita, T., Riznichenko, O.Y., Roberts, R.G., Sandoval, S.,. Sanina I.A., Sharov, N.V., Shomali, Z.H., Tiikainen, J., Wieland, E., Wylegalla, K., Yliniemi, J. and Yurov, Y.G.: Complex lithospheric structure under the central Baltic Shield from surface wave tomography, J. Geophys. Res., 109, B10303, 2004.

Bungum, H. and Lindholm, C.: Seismo- and neotectonics in Finnmark, Kola and the southern Barents Sea, part 2: Seismological analysis and seismotectonics, Tectonophysics, 270, 15-28, 1996.

Bungum, H., Olesen, O., Pascal, C., Gibbons, S., Lindholm, C., Vestøl, O. To what extent is the present seismicity of Norway driven by post-glacial rebound? Journal of the Geological Society, 167, 373-384, 2010.

Daly, J. S., Balagansky, V. V., Timmerman, M. J., and Whitehouse, M. J.: The Lapland-Kola orogen: Palaeoproterozoic collision and accretion of the northern Fennoscandian lithosphere, in: European Lithosphere Dynamics, edited by: Gee, D. G. and Stephenson, R. A., Geol. Soc. London, Mem. Ser., 32, 579–598, 2006

Eberhart-Phillips, D.: Local earthquake tomography: earthquake source regions, in Seismic Tomography: Theory and Practice, edited by H. M. Iyer and K. Hirahara, 1993.

Eken, T., Shomali, Z. H., Roberts, R. and Bödvarsson, R.. Upper-mantle structure of the Baltic Shield below the Swedish National Seismological Network (SNSN) resolved by teleseismic tomography. Geophys. J. Int., 169(2), 617-630, 2007.

Glaznev, V. N.: Complex geophysical models of the Fennoscandian lithosphere, Apatity, 252 p., (in Russian), 2003.

Отформатировано: Цвет шрифта: Красный

Guggisberg, B.: Eine zweidimensionale refraktionsseismiche interpretation der geschwindigkeits-tiefen-struktur des oberen erdmantels unter dem Fennoskandischen Schild (projekt FENNOLORA), Ph.D. thesis, Eidg. Techn. Hochsch. Zurich, Zurich, Switzerland, 1986.

Guggisberg, B., Kaminski, W., and Prodehl, C.: Crustal structure of the Fennoscandian Shield: A traveltime interpretation of the long-range FENNOLORA seismic refraction profile, Tectonophysics, 195, 105-137, doi:10.1016/0040-1951(91)90208-, 1991.

Hardebeck J.L. and Shearer, P.M.: HASH: A FORTRAN Program for Computing Earthquake First-Motion Focal Mechanisms - v1.2 - January 31, 17 p., http://quake.wr.usgs.gov/research/ software/#HASH, 2008.

Hauser, F., and Stangl, R.: The structure of the crust and the lithosphere in Fennoscandia derived from a joint interpretation of P- and S-wave data of the FENNOLORA refraction seismic profile, in Sixth EGT Workshop: Data Compilation and Synoptic Interpretation, edited by R. Freeman and S. Mueller, 71-92 pp., Eur. Sci. Found., Strasbourg, France, 1990.

Herrmann, R.B. and Ammon, C. J.: Computer programs in seismology - Source inversion, v.3-30, 98p, 2002.

Hess, H. H. "History of Ocean Basins". In A. E. J. Engel, Harold L. James, and B. F. Leonard. Petrologic studies: a volume in honor of A. F. Buddington. Boulder, CO: Geological Society of America. pp. 599-620, 1962.

Hjelt, S.-E., Korja, T., Kozlovskaya, E., Lahti, I., Yliniemi, J., and BEAR and SVEKALAPKO Working Groups: Electrical conductivity and seismic velocity structures of the lithosphere beneath the Fennoscandian Shield, in: European Lithosphere Dynamics, edited by: Gee, D. and Stephenson, R., Geol. Soc. London, Mem. Ser., 32, 2006.

Janik, T., Kozlovskaya, E., Heikkinen, P., Yliniemi, J., and Silvennoinen, H.: Evidence for preservation of crustal root beneath the Proterozoic Lapland-Kola orogen (northern Fennoscandian shield) derived from P and S wave velocity models of POLAR and HUKKA wide-angle reflection and refraction profiles and FIRE4 reflection transect, J. Geophys. Res., 114, B06308, doi:10.1029/2008JB005689, 2009.

Juhlin, C. and Lund, B.: Reflection seismic studies over the end-glacial Burtrask fault, Skelleftea, Sweden, Solid Earth, 2, 9-16, www.solid-earth.net/2/9/2011/ Solid Earth doi:10.5194/se-2-9-2011, 2011.

Kissling, E.: Geotomography with Local Earthquake Data, Rev. of Geophysics, 26, I.4, 659-698, doi: 10.1029/RG026i004p00659, 1988.

Kissling, E., Ellsworth, W. L., Eberhart-Phillips, D. and Kradolfer, U.: Initial Reference Models in Local Earthquake Ttomography, J. Geophys. Res., 99, 19, 635-646, 1994.

Koistinen, T., Stephens, M. B., Bogatchev, V., Nordgulen, Ø., Wennerström, M., and Korhonen, J.: Geological map of Fennoscandian shield, scale 1 : 2 000 000, Geological Surveys of Finland, Norway and Sweden and the North-West Department of Natural Resources of Russia, 2001.

Kuivamäki, A., Vuorela, P. & Paananen, M.. Indications of postglacial and recent bedrock movements in Finland and Russian Karelia. Geological Survey of Finland, Report YST-99, 92 p., 1998

Kukkonen I.T., Heikkinen P., Ekdahl E., Hjelt S.-E., Yliniemi J., Jalkanen, E. and FIRE Working Group: Acquisition and geophysical characteristics of reflection seismic data on FIRE transects, Fennoscandian Shield, in Finnish Reflection Experiment (FIRE) 2001-2005, edited by I. T. Kukkonen and R. Lahtinen, pp. 13-44, Geol. Surv. of Finland, Espoo, Finland, 2006.

Korja, A., Kosonen, E. (eds), Seismotectonic framework and seismic source area models in Fennoscandia, northern Europe, Report S-63, Institute of Seismology, University of Helsinki, 285 pp., 2015

Lagerbäck, R. and Sundh, M.. Early Holocene faulting and paleoseismicity in northen Sweden, Swedish Geological Survey, Research Paper C 836, 80 pp., 2008Lahr, J.C.: HYPOELLIPSE/Version 2.0: A computer program for determining local earthquake hypocentral parameters, magnitude, and first motion pattern, U.S. Geological Survey Open-File Report 89-116, 92 p, 1989.

Lahtinen R, Garde A.A. and Melezhik V.A.: Paleoproterozoic tectonic evolution of Fennoscandia and Greenland, Episodes, 31, 1-9, 2008.

Lahtinen, R., Korja, A. and Nironen, M.: Paleoproterozoic tectonic evolution in: Precambrian Geology of Finland - Key to the Evolution of the Fennoscandian Shield, edited by: Lehtinen M., Nurmi P.A. and Ramo O.T., Elsevier Science, Amsterdam , 481-531, 2005.

Lidberg, M., Jan M. Johansson, Hans-Georg Scherneck, Glenn A. Milne. Recent results based on continuous GPS observations of the GIA process in Fennoscandia from BIFROST, Journal of Geodynamics, Elsevier, 2010, 50 (1), pp.8., doi::10.1016/j.jog.2009.11.010

Lindblom, E., B. Lund, A. Tryggvason, M. Uski, R. Bödvarsson, C. Juhlin, R. Roberts Microearthquakes illuminate the deep structure of the endglacial Pärvie fault, northern Sweden, Geophys. J. Int, 201, 1704-1716, 2015.

Luosto U., Flueh E.R., Lund C.-E. and Working Group: The crustal structure along the POLAR Profile from seismic refraction investigation, Tectonophysics, 162, 51-85, doi:10.1016/0040-1951(89)90356-9, 1989.

Majdanski, M., Kozlovskaya, E. and Grad, M.: 3D structure of the Earth's crust beneath the northern part of the Bohemian Massif, Tectonophysics, 438, 1-4, 57-77, 2007.

Mikko, H., C.A. Smith, B. Lund, M.V.S. Ask, R. Munier LiDAR-derived inventory of post-glacial fault scarps in Sweden, GFF, doi: 10.1080/11035897.2015.1036360, 2010.

Nelson, G.D. and Vidale, J.E.: Earthquake locations by 3-d finite-difference travel times, Bull. Seis. Soc. Am., 80, 2, 395-410, 1990.

Olesen, O., Blikra, L.H., Braathen, A., Dehls, J.F., Olsen, L., Rise, L.., Roberts, D., Riis, F., Faleide, J.I. and Anda, E.. Neotectonic deformation in Norway and its implications: a review. Norwegian, Journal of Geology 84, 3-34, 2004.

Olsson, S., Roberts, R. and Bödvarsson, R.. Moho depth variation in the Baltic Shield from analysis of converted waves. GFF, 130, 113-122, 2008.

Pavlenkova, N.I.: Lithospheric structure of the Baltic shield from DSS data, in Structure and dynamics of the lithosphere of Eastern Europe, Geokart, Geos, Moscow, Russia, 33-58, 2006.

Plomerová, J., Vecsey, L., Babuška, V., and LAPNET Working Group: Domains of Archean mantle lithosphere deciphered by seismic anisotropy – inferences from the LAPNET array in northern Fennoscandia, Solid Earth, 2, 303–313, doi:10.5194/se-2-303-2011, 2011.

Podvin, P. and Lecomte, I.: Finite difference computation of travel times in very contrasted velocity models: a massively parallel approach and its associated tools, Geophys. J. Int. 105, 271-284, 1991.

Poli, P., Campillo, M., Pedersen, H. and the POLENET/LAPNET Working Group: Noise directivity and group velocity tomography in a region with small velocity contrasts: the northern Baltic shield application to the northern Baltic Shield, Geoph. J. Int., 192, 1, 413-424, doi: 10.1093/gji/ggs034, 2013.

Redfield, T.F., Osmundsen, P.T. The Long –term topographic response of a continent adjacent to a hyperextended margin: a case study from Scandinavia. Geological Society of America Bulletin, v. 125, p. 184-200, 2013.

Отформатировано: Цвет шрифта: Красный

Redfield, T.F., Osmundsen, P.T. Some remarks on the earthquakes of Fennoscandia: A conceptual seismological model drawn from the perspective of hyperextension, Norwegian Journal of Geology, 94, 233-262, 2015.

Sandoval, S., Kissling, E., Ansorge, J. and the SVEKALAPKO STWG: High-Resolution body wave tomography beneath the SVEKALAPKO array: I. A-priori 3D crustal model and associated travel time effects on teleseismic wavefronts, Geoph. J. Int., 153, 75-87, 2003.

Sandoval, S., Kissling, E., Ansorge, J. and the SVEKALAPKO STWG: High-Resolution body wave tomography beneath the SVEKALAPKO array: II. Anomalous upper mantle structure beneath central Baltic Schield, Geoph . J. Int., 157, 200-214, 2004.

Sharov, N. V.: Lithosphere of the Baltic Shield Based on Seismic Data (in Russian), Kola Res. Cent., Apatity, Russia, 144 pp., 1993.

Silvennoinen, H., Kozlovskaya, E., Kissling, E., Kosarev, G. and the POLENET/LAPNET Working Group: A new Moho boundary map for the northern Fennoscandian Shield based on combined controlled-source seismic and receiver function data, GeoResJ 1-2, 19-32, 2014.

Silvennoinen, H., Kozlovskaya, E., Yliniemi, J. and Tiira, T.: Wide angle reflection and refraction seismic and gravimetric model of the upper crust in FIRE4 profile area, northern Finland, Geophysica, 46, 1-2, 21-46, 2010.

Silvennoinen, H., Kozlovskaya, E. and Kissling, E.: POLENET/LAPNET teleseismic P-wave traveltime tomography model of the upper mantle beneath northern Fennoscandia, Solid Earth Discuss., 7, 2527-2562, www.solid-earth-discuss.net/7/2527/2015/, doi:10.5194/sed-7-2527-2015, 2015.

Slunga, R.S., 1991. The Baltic Shield earthquakes. In: S. Bjiimsson, S. Gregersen, E.S. Husebye, H.Korhonen & C.-E. Lund (Eds.), Imaging and Understanding the Lithosphere of Scandinavia and Iceland. Tectonophysics, 189: 323-3111.

Stammler K.: SeismicHandler - programmable multichannel data handler for interactive and automatic processing of seismological analyses, Comp. Geosciences, 19, 135-140, 1993.

Steffen, R., Steffen, H., Wu, P. and Eaton, D. W.: Stress and fault parameters affecting fault slip magnitude and activation time during a glacial cycle, Tectonics, 33, 1461-1476, doi:10.1002/2013TC003450, 2014.

Sutinen, R., Hyvönen E., Middleton, M., Ruskeeniemi, T. Airborne LiDAR detection of postglacial faults and Pulju moraine in Palojärvi, Finnish Lapland. Global and Planetary Change 115, 24-32, 2014.

448 Talbot C.J. : Weak zones in Precambrian Sweden, Geological Society, London, Special Publications; v. 186; p. 287-304,
449 doi:10.1144/GSL.SP.2001.186.01.17, 2001.

450 Thurber, C. H.: Earthquake locations and three-dimensional crustal structure in the Coyote Lake area, central California, J. Geophys. Res., v. 88, p. 8226-
451 8236, 1983.

452 Thurber, C. H.: Local earthquake tomography: velocities and Vp/Vs - theory, in Seismic Tomography: Theory and Practice, edited by H. M. Iyer and K.
453 Hirahara, 1993.

454 Uski M., Hyvonen, T., Korja, A., Airo, M.: Focal mechanisms of three earthquakes in Finland and their relation to surface faults, Tectonophysics, 363, 141
455 - 157, 2003.

456 Uski, M., Korja, A., 2007. Hypocenter distribution of earthquakes in north-western Finnish Lapland: preliminary investigation. Abstract in: The 38th
457 Nordic Seismology Seminar, Helsinki, 12-15.6.2007

458 Usoltseva O., Kozlovskaya, E., Konstantinovskaya, N. and POLENET/LAPNET Working Group Team: Intraplate seismicity in northern Fennoscandia
459 from data of the POLENET/LAPNET experiment, Proceedings of the 9th International Conference PROBLEMS OF GEOCOSMOS, editors: V. N.
460 Troyan, V. S. Semenov, M. V. Kubyshkina ISBN 978-5-9651-0685-1, CD disk, October 08-12, Saint-Petersburg State University (SPBU), Saint-
461 Petersburg, Russia, p.176-181, 2012.

462 Van Lanen, X and Mooney, W.D.: Integrated geologic and geophysical studies of North American continental intraplate seismicity, in Continental
463 Intraplate Earthquakes: Science, Hazard and Policy Issues, edited by Stein, S., Mazotti, S., Geological Society of America Special Paper, 425, p. 101-112,
464 doi: 10.1130/2007.2425(08) , 2007.

465 Vinnik, L., Oreshin, S., Makeyeva, L., Peregoudov, D., Kozlovskaya, E., and POLENET/LAPNET Working Group: Anisotropic lithosphere under the
466 Fennoscandian shield from P receiver functions and SKS waveforms of the POLENET/LAPNET array, Tectonophysics, 628, 45-54, 2530- 2539, 2014.

467 Virieux, J., Farra, V. and Madariaga, R.: Ray tracing in laterally heterogeneous media for earthquake location, Journal of geophysical research, 93, 6585-
468 6599, 1988.

Walther, C. and Fluh, E. R.: The POLAR profile revisited: Combined P- and S- wave interpretation, Precambrian Res., 64, 153- 168, doi:10.1016/0301-9268(93)90073-B, 1993.

Wu, P., Johnston, P. and Lambeck K.: Postglacial rebound and fault instability in Fennoscandia, Geophys. J. Int. 139, 657-670, 1999.

Table and Figure captions.

Table 1 1-D P-wave and S-wave velocity models.

Table 2 Results of Hukkavaara explosions location with using of HYPOELLIPS method (index 1) and grid search method (index 2). Sec1/2 – final source time defined by HYPOELLIPS /by grid search method, lat1/2 (lon1/2) – final latitude (longitude) defined by HYPOELLIPS /by grid search method. Dep1/2 – depth defined by HYPOELLIPS /by grid search method, RMS1 – final HYPOELLIPS root-mean-square residual, RMS2 – final grid search method RMS, , N –number of POLENET/LAPNET stations used, σ_x and σ_z - the horizontal and the vertical uncertainties at the 68 per cent confidence level, r_{min} – epicentre distance up to nearest station, r_{max} – epicentre distance up to farthest station.

Table 3 Results of events location with using of HYPOELLIPS method (index 1) and grid search method (index 2). Sec, lan, lon, dep FENCAT are the information from FENCAT. The N P.st. –number of observations in permanent POLENET/LAPNET stations, N T.st. number of observations in temporary POLENET/LAPNET stations. Sta on r_{min} –the name of nearest station. The stars are denoted the events with one and more stations satisfying the condition $\Delta<2*depth$. The rest notations are as in Table 2.

Table 4 Source parameters of selected event.

Table 5 Information about focal mechanisms of local earthquakes for Region 2 from other sources.

Figure 1 a) Location of 56 POLENET/LAPNET stations (black squares – permanent, black triangles - temporary), imposed in topographic map ETOPO1 (Amante and Eakins, 2009, http://maps.ngdc.noaa.gov/viewers/wcs-client/), b) The geological map, based on a 1:2,000,000 geological map of Fennoscandia (Koistinen et al. 2001), c) Large scale map for demonstration where the study area is located in Fennoscandia. Red lines (in map b with red numerals) are denoted postglacial faults (Sutinen et al. 2014, Mikko et al. 2015): 1 - Palojärvi, Paatsikkajoki and Kultima, 2 - Lainio-Suijavaara, 3 – Merasjärvi, 4 – Lansjärv, 5 – Venejärvi, Ruostejärvi and Pasmajärvi, 6 – Isovaara, 7 –

Suasselkä. Blue boxes – investigation Regions 1 and 2. Region 1 is the region for tomographic research and Region 2 is the region for reliable location. Blue dotted line - profile HUKKA S.

Figure 2 a) Epicentres of 34 local earthquakes, graded according Table 3 (circles are shallow earthquakes, triangles are deep earthquakes, stars are the events near the surface, crosses are the events with non stability location), used for relocation, b) Epicentres of 36 local earthquakes (circles), and 9 local explosions (stars), used for local seismic tomography. Epicentres are given according to FENCAT catalogue. The size of circles is proportional to hypocentre depth. Ev1 - event from Table 4 with determined focal mechanisms. Blue boxes – investigation Regions 1 and 2. Red lines are denoted postglacial faults.

Figure 3 Examples of waveforms of local events in Z-component: (a) shallow event 19.01.2008 19:52 67.23N 23.80E, depth=10.4 km, ML=2.2 (FENCAT), (b) deep event 03.10.2007 12:26 67.42N 22.81E, depth=27.4 km, ML=1.6 (FENCAT), (c) explosion in the Hukkavaara hill 24.08.2008 12:30 67.94N 25.79E, ML=1.1 (FENCAT). Epicentral distances Δ were calculated using FENCAT catalogue. Recordings were band-pass filtered with corner frequencies at 1 and 15 Hz and amplitude-normalized.

Figure 4 Ray propagation in 1-D layered model for shallow event. Lower panel: the rays through the model. Upper panel: the reduced calculated and picked first P-wave travel times.

Figure 5 Ray propagation in 1-D layered model for deep event. Lower panel: the rays through the model. Upper panel: the reduced calculated and picked first P-wave travel times.

Figure 6 Seismograms of explosion 16.08.2007 08:00 67.93N 25.82E ML=1.5 (FENCAT) from Hukkavaara hill. Traces are normalized to maximum amplitude.

Figure 7 Result of relocation by HYPOELLIPSE: comparison of observed and calculated travel times for shallow earthquake 19.01.2008 19:52 67.23N 23.80E, depth=10.4 km, ML=2.2 (FENCAT). Left panel demonstrates travel times before relocation, right panel shows travel times after relocation.

512 Figure 8 Result of relocation by HYPOELLIPSE: comparison of observed and calculated travel times for deep earthquake on 12.03.2009
513 22:42 67.41N 23.67E, depth=12.4 km, ML=1.0 (FENCAT). Left panel demonstrates travel times before relocation, right panel shows travel
514 times after relocation.

515 Figure 9 Event 09.06.2007 02:52 UTC 68.68N 23.30E, depth=26.7 km, ML=1.7 (FENCAT) a) and b) the reduced calculated and picked travel
516 times for P and S waves. c) Seismograms for the event without filtering, d) map of stations and event.

517 Figure 10 Seismograms for shallow event Ev1 from Table 4 showing the first motions for different resampling: a) 50 Hz, b) 80 Hz c) 100 Hz.
518 The traces are aligned relatively to the first P arrival.

519 Figure 11 Left: Lower hemisphere equal area projections of the focal sphere. For the polarities, octagons and triangles represent compressions
520 and dilatations. Letter symbols indicate the position of compressional (P) and tensional (T) axes. Middle: the set of 150 acceptable
521 mechanisms. Right: the distributions of acceptable dip, rake and strike for these solutions.

522 Figure 12 The time station corrections imposed in topographic map ETOPO1 (Amante and Eakins, 2009) and computed with respect to the
523 reference station HEF by VELEST. Stars are denoted negative corrections, snowflakes are denoted positive corrections. The size of the sign
524 (star or snowflake) is proportional to value of correction.. The red lines are denoting post-glacial faults. Blue box indicates investigation
525 Region 1. The full names of faults are the same as in Fig. 1b.

526 Figure 13 The ray coverage of the area in the horizontal and two vertical planes.

527 Figure 14 Results of the checkerboard test for checks a) 75*75 km, b) 100*100 km. Horizontal cross sections of the reconstructed pattern are
528 shown for depths 1.3, 10.0 and 18.0 km. The dotted lines are the boundaries of synthetic checks with different velocity in testing model. Green
529 contour restrict the area with resolution more than 0.5.

530 Figure 15 Results of synthetic checkerboard test for checks of 150*75 km: a) orientation of synthetic checks is normal, orientation of grid is
531 normal, b) orientation of synthetic checks is normal, orientation of grid is turned at angle of 30^0 counter clockwise from the North, c)

orientation of synthetic checks is turned, orientation of grid is normal, d) orientation of synthetic checks is turned, orientation of grid is turned. The other descriptions are the same as in Fig. 13.

Figure 16 Upper crustal 3-D velocity structure of the Region 1 reconstructed with SIMULPS14 and appropriate isolines of velocity anomalies on the background of the geological map. Horizontal cross sections for depths: 1.3, 10.0, 18.0 km a), b) for usual grid and c), d) for grid, oriented at angle of 30^0 counter clockwise from the North. Green contour restrict the area with resolution more than 0.5. Yellow lines are denoted post-glacial faults (detailed in Fig.1). Black lines are denoted profiles: FIRE with letter F, POLAR with letter P. Black points are the relocated in 3D model earthquakes in section 1.8 km with depths<6 km, in section 10 km with 6≤depths<14 km, in section 18 km with depths≥14 km. Black blank circles are the explosions in section 1.8 km.

Figure 17 Local earthquakes from catalogue FENCAT in the period with 1964 to 2008 years in the Region 2. The earthquakes are divided in 5 groups depending on hypocentre depth. The number of earthquakes equals 55 in 1 group, 126 in 2 group, 17 in 3 group, 21 in 4 group, 4 in 5 group. Brown lines are denoting post-glacial faults. Baltic-Bothnia Megashear (BBMS) from (Berthelsen and Marker, 1986) is shown by yellow stripe.

Figure 18 Available fault plane solutions for the earthquakes in Region 2 (lower hemisphere equal area projection): black circles show events from Table 6. Deep earthquakes with reliable location from Table 3 are shown by purple circles. Events for which we calculated focal mechanisms (Table 4) are indicated by brown circle. Brown lines are denoting post-glacial faults (details in Fig. 1). BBMS from (Berthelsen and Marker, 1986) is shown by yellow stripe.

549

550 Tables.

551 **Table 1** 1-D P-wave and S-wave velocity models.

layer (km)	**Vp (km s^{-1})**	**Vp*Vs^{-1}**	Vs (km s^{-1})
0-1.3	6.2	1.71	3.63
1.3-18	6.3	1.72	3.66
18-37	6.6	1.72	3.84
37-40	7.15	1.79	3.99
40-44	7.4	1.82	4.07
44-50	8.03	1.73	4.64
Upper 50	8.4	1.73	4.86

552

*T*able 2 Results of Hukkavaara explosions location with using of HYPOELLIPS method (index 1) and grid search method (index 2). Sec1/2 – final source time defined by HYPOELLIPS /by grid search method, lat1/2 (lon1/2) – final latitude (longitude) defined by HYPOELLIPS /by grid search method. Dep1/2 – depth defined by HYPOELLIPS /by grid search method, RMS1 – final HYPOELLIPS root-mean-square residual, RMS2 – final grid search method RMS, , N –number of POLENET/LAPNET stations used, σ_x and σ_z - the horizontal and the vertical uncertainties at the 68 per cent confidence level, r_{min} – epicentre distance up to nearest station, r_{max} – epicentre distance up to farthest station.

Yy m dd	hh:mi	sec1/ sec2	lat ^{0}N ½	lon ^{0}E ½	dep (km)1/2	RMS1 (s)	RMS2 (s)	Gap (deg)	N	σ_x (km)	σ_z (km)	r_{min} (km)	r_{max} (km)
08 08 24	12:30	0.9/ 0.8	67.95/67.94	25.82/25.83	0.2/ 0.0	0.13	0.18	47	25	0.3	0.9	24	267
08 08 29	11:00	0.5/ 0.4	67.93/67.94	25.83/25.85	0.0/ 0.0	0.25	0.23	47	23	0.7	4	25	179
07 08 16	08: 00	0.4/ 0.4	67.94/67.94	25.82/25.85	0.0/ 0.05	0.18	0.13	117	7	0.6	3	59	239

559 Table 3 Results of events location with using of HYPOELLIPS method (index 1) and grid search method (index 2). Sec, lan, lon, dep
560 FENCAT are the information from FENCAT. The N P.st. –number of observations in permanent POLENET/LAPNET stations, N T.st.
561 number of observations in temporary POLENET/LAPNET stations. Sta on r_{min} –the name of nearest station. The stars are denoted the events
562 with one and more stations satisfying the condition $\Delta<2*depth$. The rest notations are as in Table 2.

yy.mm.dd	hh:mi UTC	Sec FENCAT	sec1/sec2	lat ^{0}N FENCAT	lat ^{0}N ½	lon ^{0}E FENCAT	lon ^{0}E 1/2	Dep FENCAT	dep (km)1/2	RMS (s)1	RMS (s)2	Gap (deg)	N P.st.	N T.st	σ_x (km)	σ_z (km)	r_{min} (km)	Sta on r_{min}
Events with non stability location																		
071128	4:14	45.1	44.7/44.6	67.42	67.39/67.40	24.35	24.32/24.32	2.0F	1.9/ 0.5	0.21	0.16	158	5	17	0.4	22.4	33.6	lp41
080531	7:17	29.9	30.1/30.1	67.03	67.03/67.03	24.07	24.04/24.08	1.5	3.1/10.5	0.34	0.4	48	15	10	0.7	10.6	16.6	lp41
Events with stability location																		
Shallow earthquakes (depth less 20 km)																		
070702	3:04	10.1	10.1/10.1	68.05	68.05/68.05	22.82	22.81/22.83	8.5	10.1/ 9.5	0.27	0.28	67	13	8	0.2	0.4	34.1	lan
070716*	22:43	0.3	0.6/ 0.3	68.50	68.49/68.50	23.74	23.74/23.73	6.6	7.3/ 9.5	0.26	0.11	102	8	6	0.7	3	9.5	hef
070917*	1:50	41.5	41.3/41.4	68.41	68.42/68.42	23.32	23.31/23.31	11.5	12.9/12.5	0.23	0.2	107	5	11	0.9	1.2	14.6	hef
070920	20:38	39.8	39.5/39.7	67.89	67.86/67.88	22.63	22.60/22.62	1.0F	5.4/ 5.5	0.35	0.26	177	6	15	0.6	2.2	56.2	lp61
071013	15:29	2.3	2.5/ 2.5	67.68	67.69/67.69	24.76	24.77/24.80	5.0F	3.4/ 2.5	0.22	0.21	64	5	20	0.6	4.7	18.2	lp52
071128	4:39	41.9	41.6/41.7	67.42	67.38/67.39	24.28	24.25/24.30	1.4	10.5/ 9.5	0.29	0.21	163	5	16	1	3.1	33	lp41
071207*	20:38	48.5	48.6/48.6	67.10	67.10/67.10	25.81	25.78/25.80	7.6	5.7/ 8.5	0.27	0.24	64	7	24	0.4	1.5	9.1	lp42
080119	19:52	3.0	3.0/ 3.0	67.23	67.25/67.26	23.80	23.77/23.79	10.4	11.3/10.5	0.21	0.2	37	15	30	0.3	0.9	23.6	lp51
080126	5:32	29.4	29.5/29.5	68.08	68.10/68.10	23.46	23.47/23.50	14.9	14.5/14.5	0.26	0.26	92	6	17	0.2	0.4	28	lp61
080420	18:31	18.9	19.0/18.9	66.92	66.92/66.92	23.64	23.61/23.63	6.0	9.0/12.5	0.27	0.25	52	14	14	0.7	2.6	24.9	paj
080607	11:33	22.2	22.4/22.3	68.83	68.83/68.83	23.67	23.66/23.68	7.0	5.4/ 4.5	0.34	0.35	59	13	13	1.5	5.7	26.7	ktk1
080719	19:11	19.1	19.1/19.1	67.96	67.95/67.97	22.78	22.79/22.81	5.2	6.3/ 6.5	0.36	0.33	80	17	14	0.6	1.7	35.2	lan
080830	4:48	49.6	49.5/49.5	67.74	67.74/67.74	22.79	22.77/22.80	5.0F	6.4/ 7.5	0.39	0.36	75	21	11	0.4	3.3	45	mas
080913*	7:21	10.5	10.4/10.6	68.20	68.19/68.20	23.81	23.80/23.83	4.7	11.7/ 9.5	0.37	0.31	47	15	31	0.4	0.7	24.3	hef
081023	18:41	9.7	9.5/ 9.4	67.67	67.66/67.64	22.14	22.14/22.15	8.7F	15.0/12.5	0.4	0.59	63	11	10	2	5	44.2	lan
090120*	11:32	21.6	20.4/20.5	67.60	67.54/67.54	22.31	22.17/22.16	10.0	5.9/ 8.5	0.35	0.32	118	19	3	1.3	2.8	11.3	mas
090207*	9:39	8.2	8.3/ 8.3	67.39	67.39/67.40	23.55	23.54/23.56	5.0	8.7/ 8.5	0.25	0.26	37	21	21	0.5	0.8	8.2	lp51
090215	0:38	55.2	55.0/55.2	67.66	67.65/67.66	22.37	22.40/22.43	4.3F	11.6/ 6.5	0.33	0.23	119	11	13	0.4	1.4	26.9	mas
090401	23:51	46.1	46.4/46.2	67.10	67.09/67.09	25.81	25.78/25.80	5.0F	2.2/ 0.5	0.31	0.29	65	5	17	0.2	1.7	8.5	lp42
090411	3:23	16.3	16.5/16.4	67.14	67.13/67.14	25.86	25.84/25.87	4.9	0.1/ 6.5	0.39	0.38	30	19	40	0.2	2.6	13.3	lp42

090425	10:32	45.3	45.7/45.6	68.55	68.54/68.55	23.37	23.36/23.38	6.2	9.0/ 8.5	0.3	0.29	55	13	16	0.6	1.4	19.9	hef
090504*	22:45	44.8	44.9/44.9	67.41	67.42/67.41	23.57	23.57/23.56	1.4	5.5/ 4.5	0.43	0.35	45	17	10	0.3	0.6	5	lp51
090505	18:22	14.4	14.5/14.5	67.92	67.93/67.94	23.27	23.29/23.28	4.4	12.3/11.5	0.26	0.24	54	18	15	0.3	0.8	27	lp61
Events near the surface																		
071112	3:37	31.5	31.6/31.4	66.67	66.67/66.68	25.88	25.86/25.89	10.F	0.0/ 0.5	0.74	0.74	56	14	24	0.1	1.9	9.3	rnf
080212	3:41	12.0	11.7/11.6	66.94	66.93/66.93	24.14	24.05/24.06	5.8	0.0/ 0.5	0.25	0.25	166	7	25	0.4	2.1	22.8	lp41
Deep earthquakes (depth more 20 km)																		
070609*	2:52	40.3	41.8/41.8	68.68	68.72/68.75	23.30	23.09/23.11	26.7	53.4/53.5	0.56	0.47	122	9	12	0.4	0.8	32.7	ktk1
071003*	12:26	40.8	40.6/40.5	67.42	67.44/67.45	22.81	22.84/22.85	27.4	26.1/26.5	0.39	0.38	95	10	14	0.2	0.3	47.9	paj
080326*	10:55	36.4	36.2/36.4	66.67	66.68/66.70	22.88	22.88/22.91	26.5	31.9/31.5	0.24	0.22	118	10	12	0.4	0.8	33.9	ert
080922*	14:30	8.4	8.3/ 8.3	67.86	67.86/67.87	23.58	23.55/23.56	21.8	27.7/26.5	0.23	0.22	61	15	21	0.6	0.7	16.9	lp61
081109	17:00	42.0	41.9/42.0	66.59	66.59/66.59	22.96	22.95/22.99	21.4	23.9/21.5	0.46	0.37	75	22	26	0.8	1.6	50.5	lp31
090129*	22:20	35.5	35.4/35.5	69.00	69.00/69.01	23.81	23.78/23.82	33.5	34.5/31.5	0.71	0.6	108	16	20	1.1	1.5	21.8	ktk1
090312*	22:42	35.1	35.0/35.2	67.41	67.39/67.38	23.67	23.60/23.59	12.4	30.4/29.5	0.38	0.34	58	12	14	0.5	0.5	7.7	lp51

563

564

565 Table 4 Source parameters of selected event.

	Event 1
Date	13 Sept 2008
Origin time (GMT)	07:21:10.6
Latitude (^{0}N)	68.20
Longitude(^{0}E)	23.83
Depth (km)	9.5
ML	1.9
Strike/dip/rake (deg)	21/77/152
Fault plane uncertaintly (deg)	19
2 Strike/dip/rake (deg)	118/63/15
Auxiliary plane uncertaintly (deg)	24
P-axis: trend/plunge	72/9
T-axis: trend/plunge	336/29

566

567 Table 5 Information about focal mechanisms of local earthquakes for Region 2 from other sources.

№	data	Ml	depth	lat	lon	strike	dip	rake	Source
1	1987/05/27	2.0	14.0	66.64	22.37	30	80	34	(Arvidsson, 1996)
2	1987/07/18	2.4	34.0	66.42	21.71	205	70	20	(Arvidsson, 1996)
3	1989/11/16	1.6	12.5	68.83	23.67	0	90	0	(Bungum and Lindholm, 1996)
4	2001/05/02	2.9	5.0	67.16	24.59	35	30	90	(Uski et al., 2003)
5	2007/01/16	1.5	21.9	68.38	23.73	193	57	66	(Uski and Korja, 2007)
6	2007/02/25	1.3	8.6	68.47	23.69	191	56	78	(Uski and Korja, 2007)
7	1989/01/09	1.7		69.46	24.64	45	30	70	(Bungum and Lindholm, 1996)
8	1991/04/13	2.6	10.0	69.12	24.05	30	45	120	(Bungum and Lindholm, 1996)
9	1996/01/21	3.8	12.8	69.4	23.4	174	53	64	(Bungum and Lindholm, 1996)
10	1975/08/11	3.9		67.4	21.76	350	85	-90	(Arvidsson and Kulhanek, 1994)

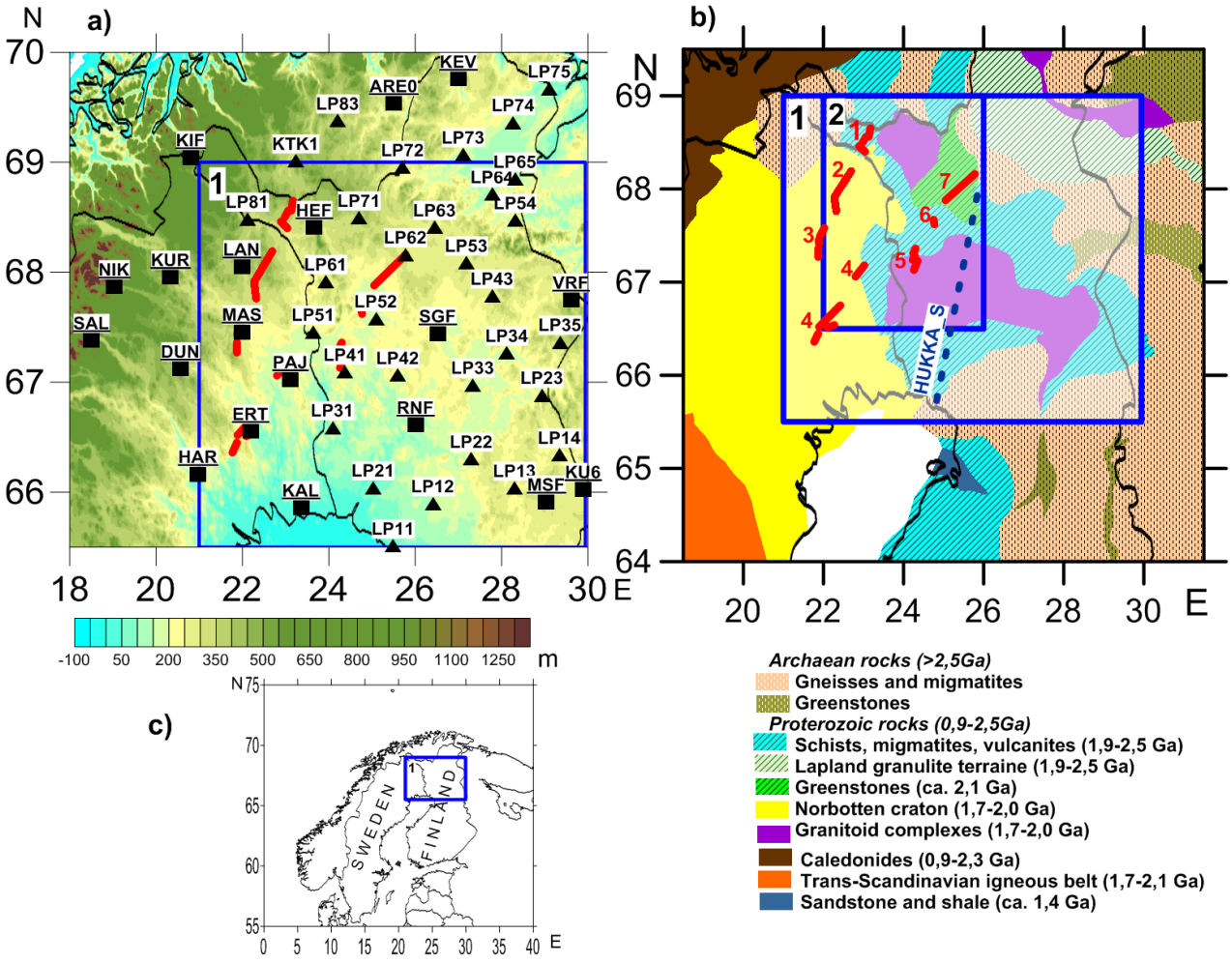
a)
b)
c)
N
70
69
68
67
66
18
20
22
24
26
28
30
E
KEV
LP75
ARE0
LP83
LP74
KIF
KTK1
LP72
LP73
LP65
LP64
LP81
HEF
LP71
LP63
LP54
LAN
LP62
LP53
NIK
KUR
LP61
LP43
VRF
LP52
SAL
MAS
LP51
SGF
LP34
LP35
DUN
PAJ
LP41
LP42
LP33
LP23
ERT
LP31
RNF
LP22
LP14
HAR
LP21
LP13
KU6
KAL
LP12
MSF
LP11
-100
50
200
350
500
650
800
950
1100
1250
m
69
68
67
66
65
64
20
22
24
26
28
30
E
HUKKA S
Archaean rocks (>2,5Ga)
Gneisses and migmatites
Greenstones
Proterozoic rocks (0,9-2,5Ga)
Schists, migmatites, vulcanites (1,9-2,5 Ga)
Lapland granulite terraine (1,9-2,5 Ga)
Greenstones (ca. 2,1 Ga)
Norbotten craton (1,7-2,0 Ga)
Granitoid complexes (1,7-2,0 Ga)
Caledonides (0,9-2,3 Ga)
Trans-Scandinavian igneous belt (1,7-2,1 Ga)
Sandstone and shale (ca. 1,4 Ga)
N
75
70
65
60
55
0
5
10
15
20
25
30
35
40
E
SWEDEN
FINLAND

Figure 1

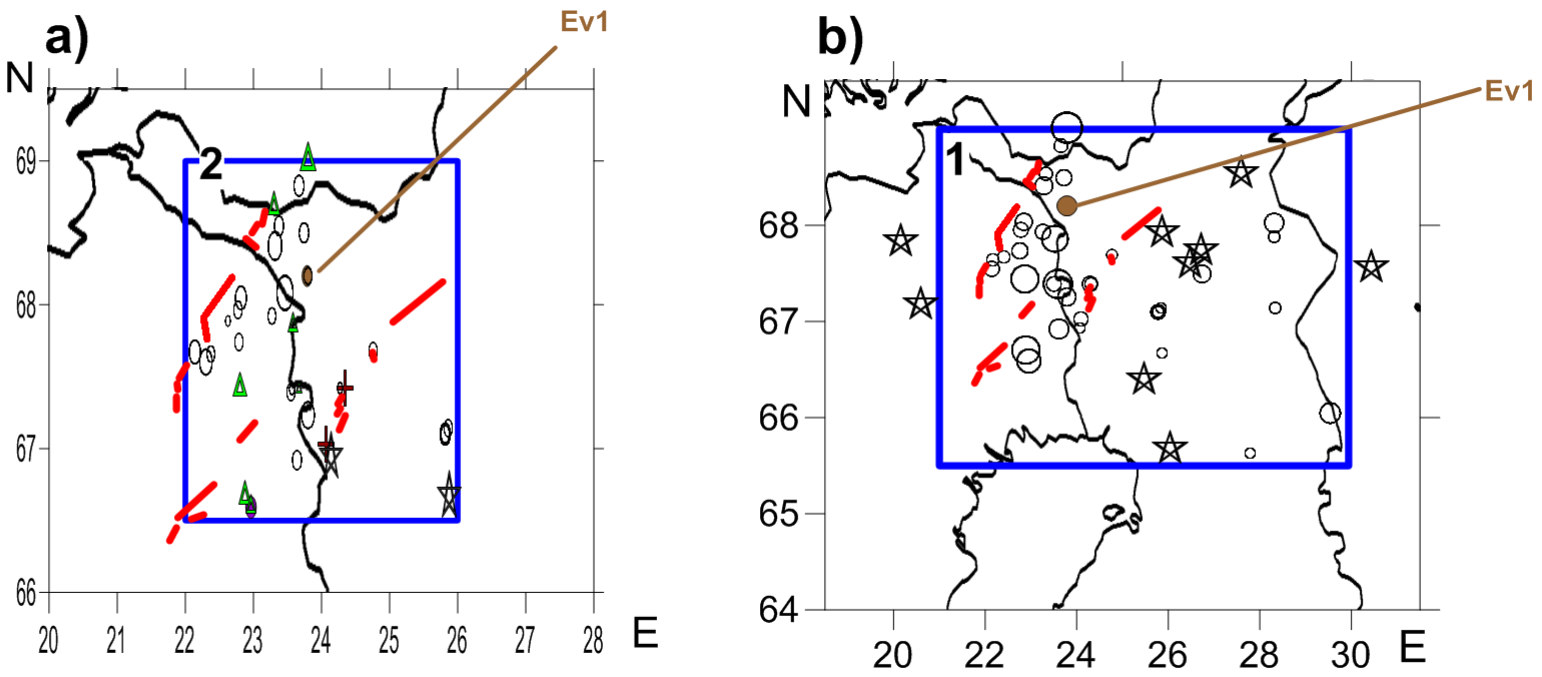

570

571 **Figure 2**

572

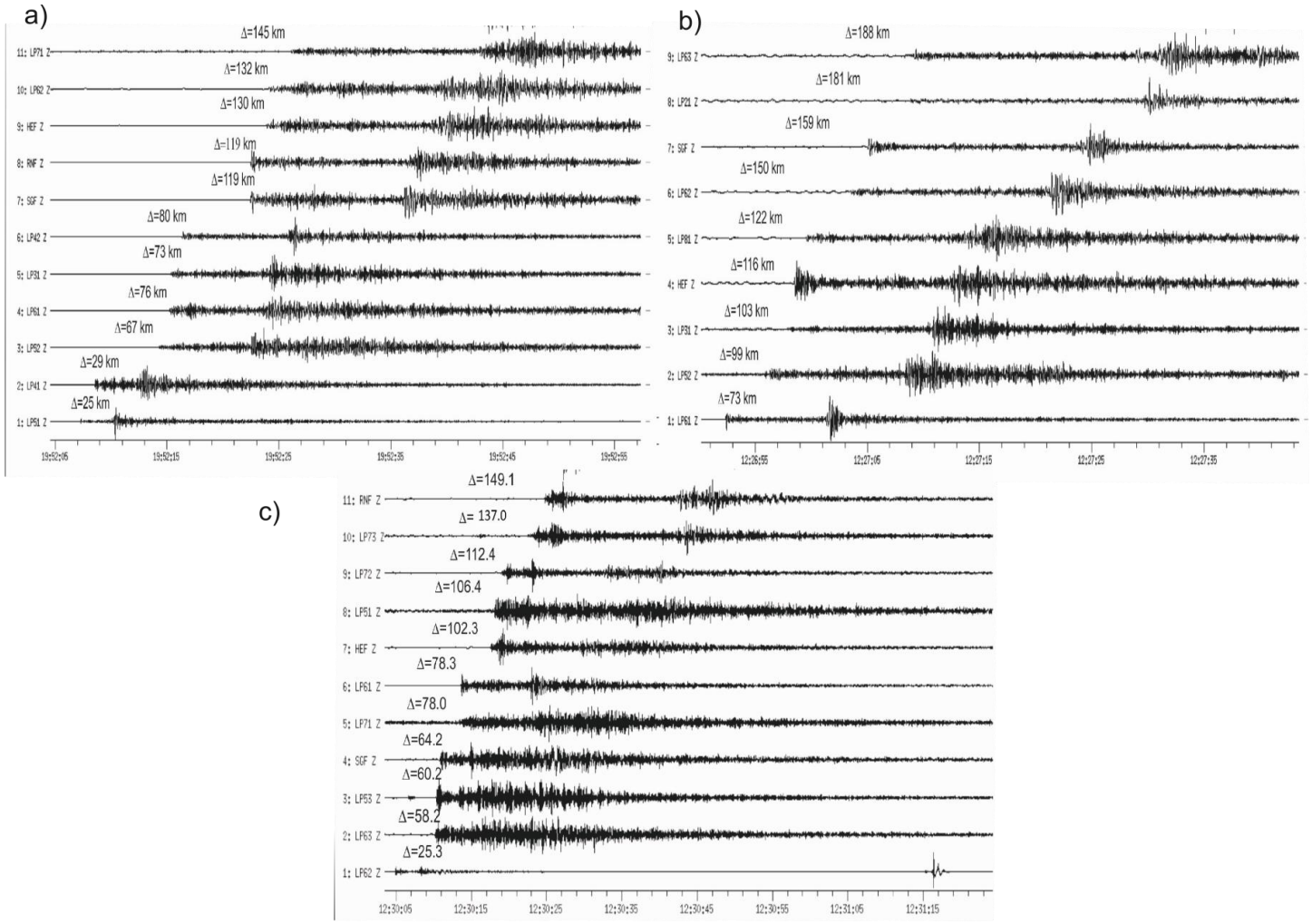

573

574 **Figure 3**

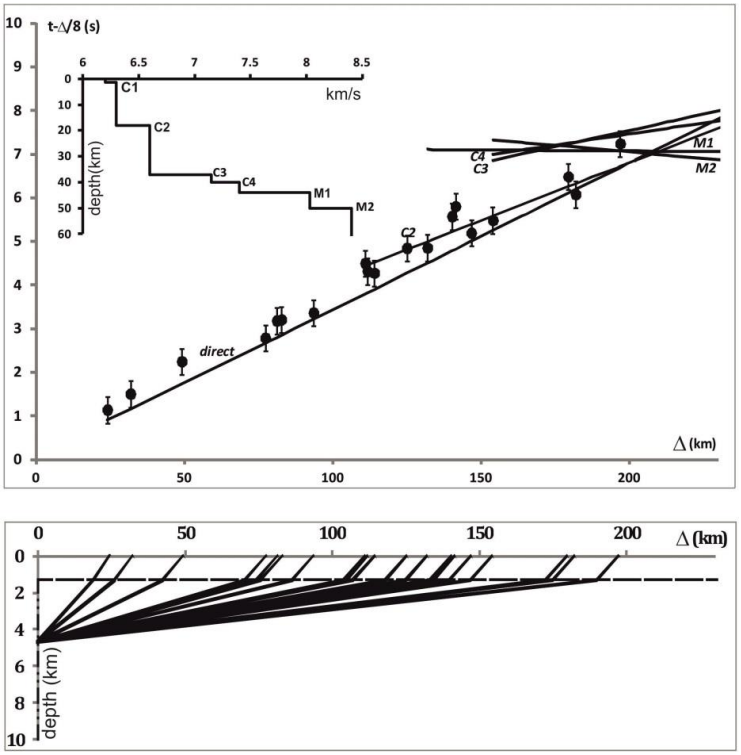

Figure 4

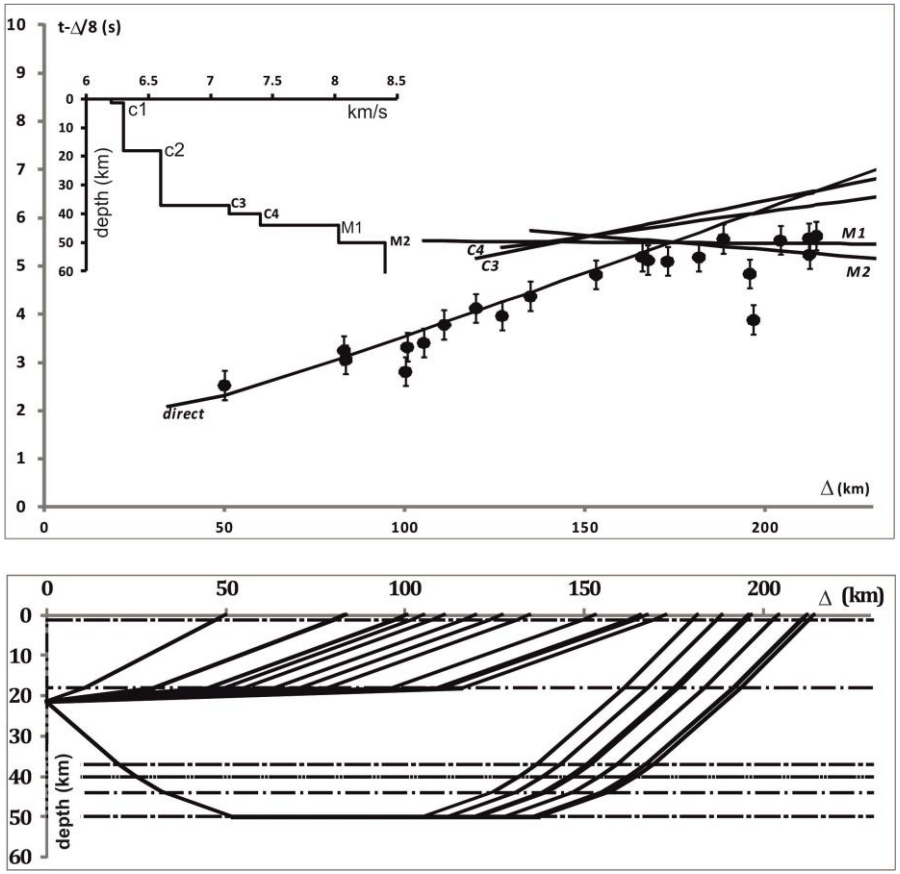

Figure 5

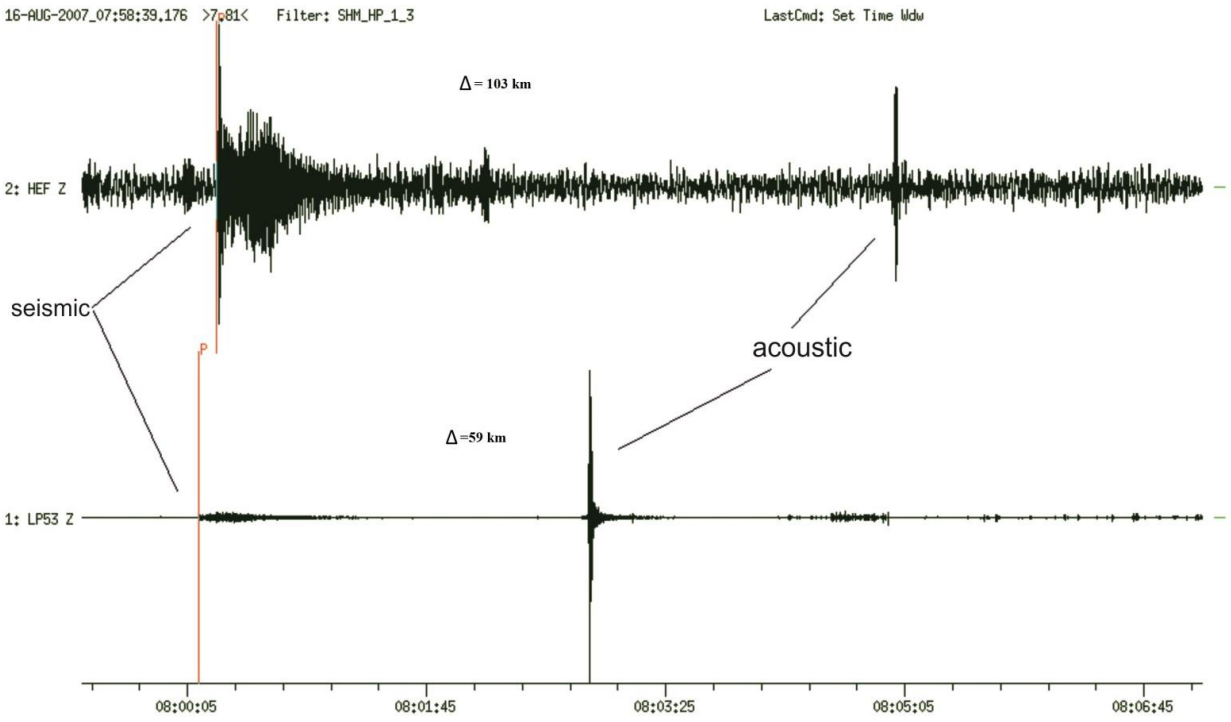

581

582 **Figure 6**

583

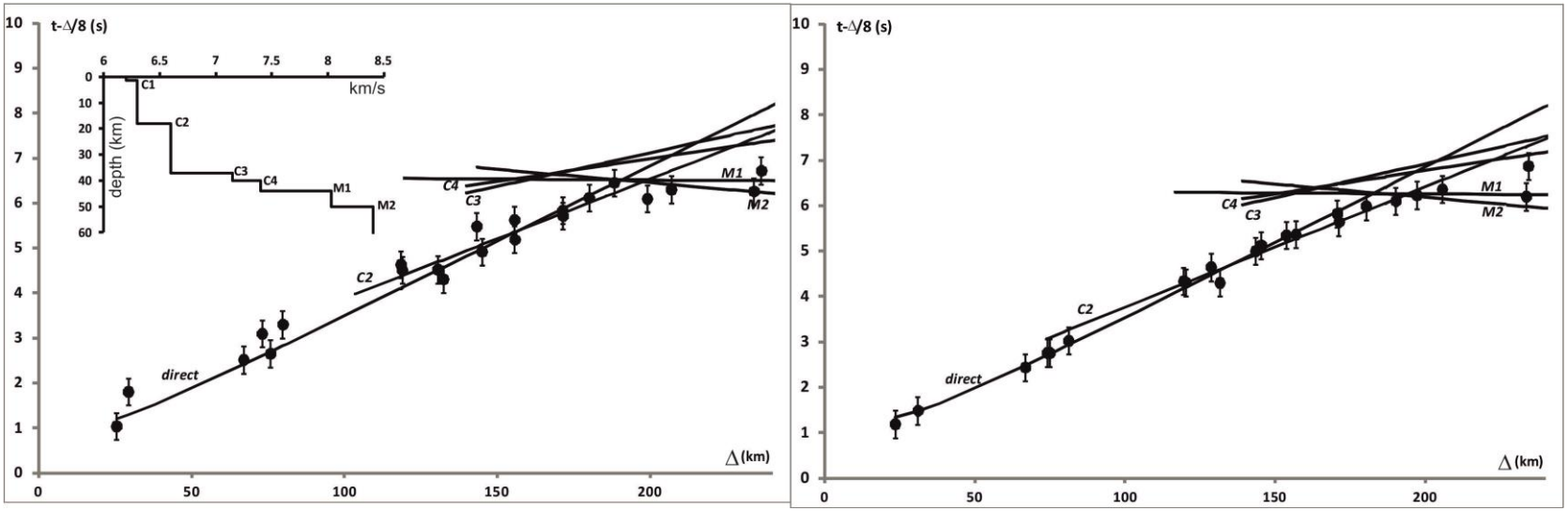

Figure 7

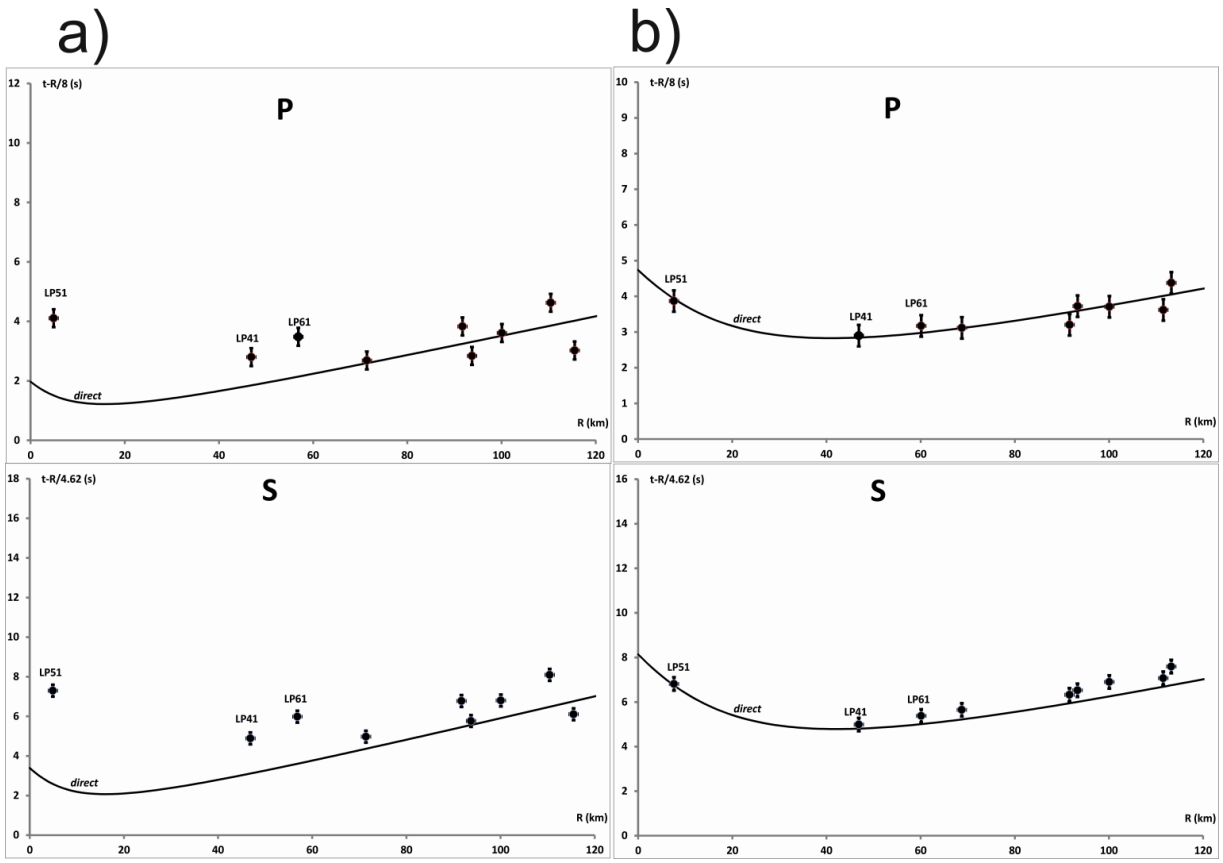

Figure 8

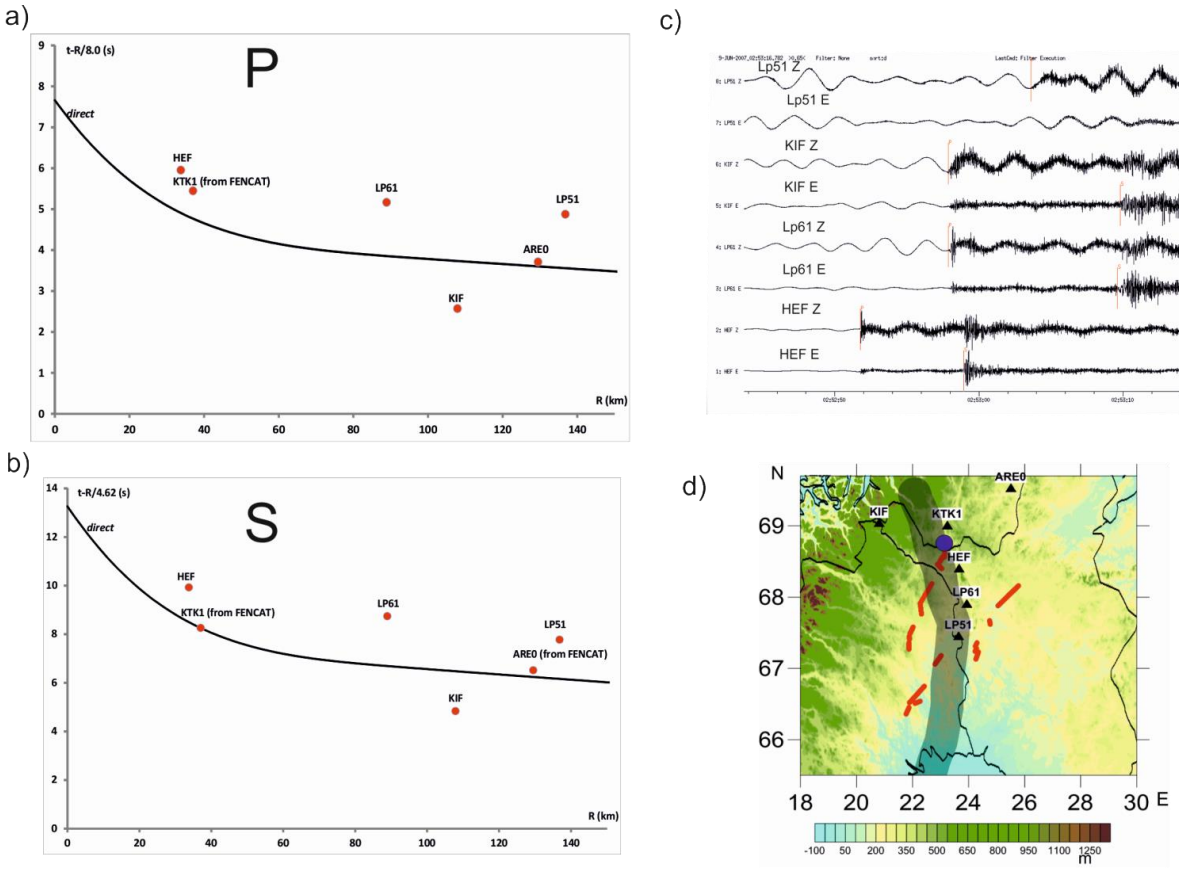
a)
t-R/8.0 (s)
P
direct
HEF
KTK1 (from FENCAT)
LP61
LP51
ARE0
KIF
R (km)
b)
t-R/4.62 (s)
S
direct
HEF
KTK1 (from FENCAT)
LP61
LP51
ARE0 (from FENCAT)
KIF
R (km)
c)
Lp51 Z
Lp51 E
KIF Z
KIF E
Lp61 Z
Lp61 E
HEF Z
HEF E
d)
N
ARE0
KIF
KTK1
HEF
LP61
LP51
69
68
67
66
18
20
22
24
26
28
30 E
-100 50 200 350 500 650 800 950 1100 1250
m

Figure 9

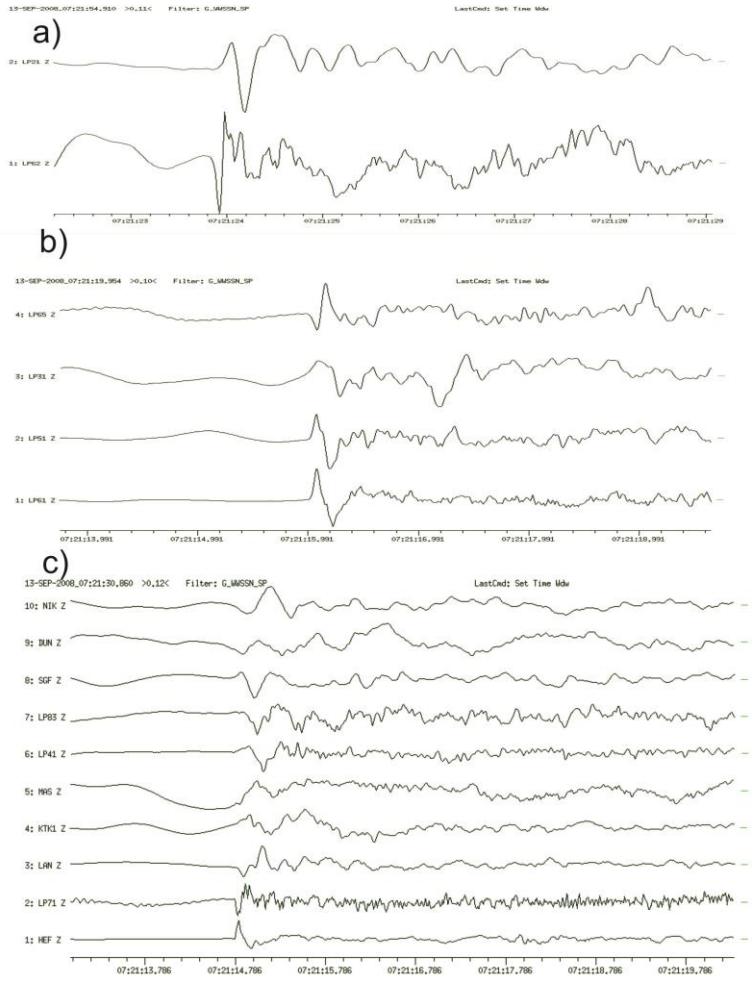
a)
b)
c)
10: NIK Z
9: DUN Z
8: SGF Z
7: LP83 Z
6: LP41 Z
5: MAS Z
4: KTK1 Z
3: LAN Z
2: LP71 Z
1: HEF Z

Figure 10

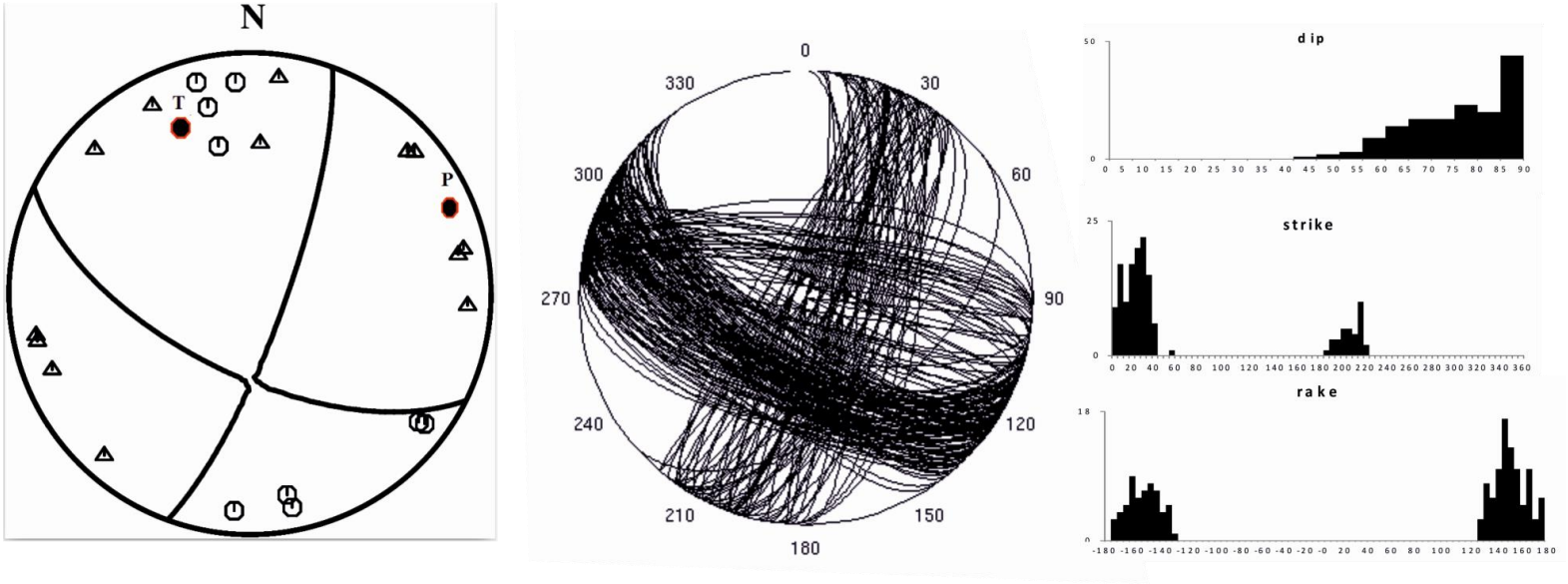

596

597 **Figure 11**

598

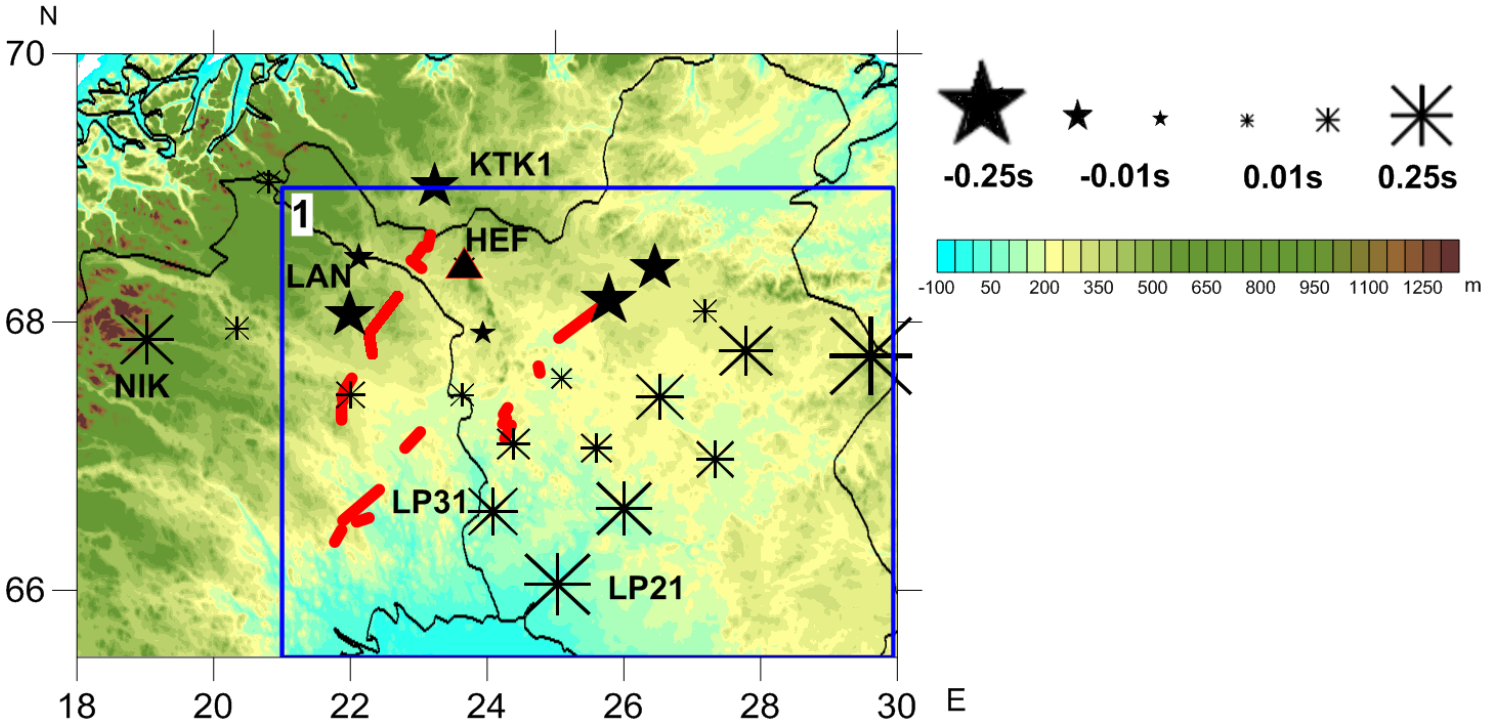

599

600 **Figure 12**

601

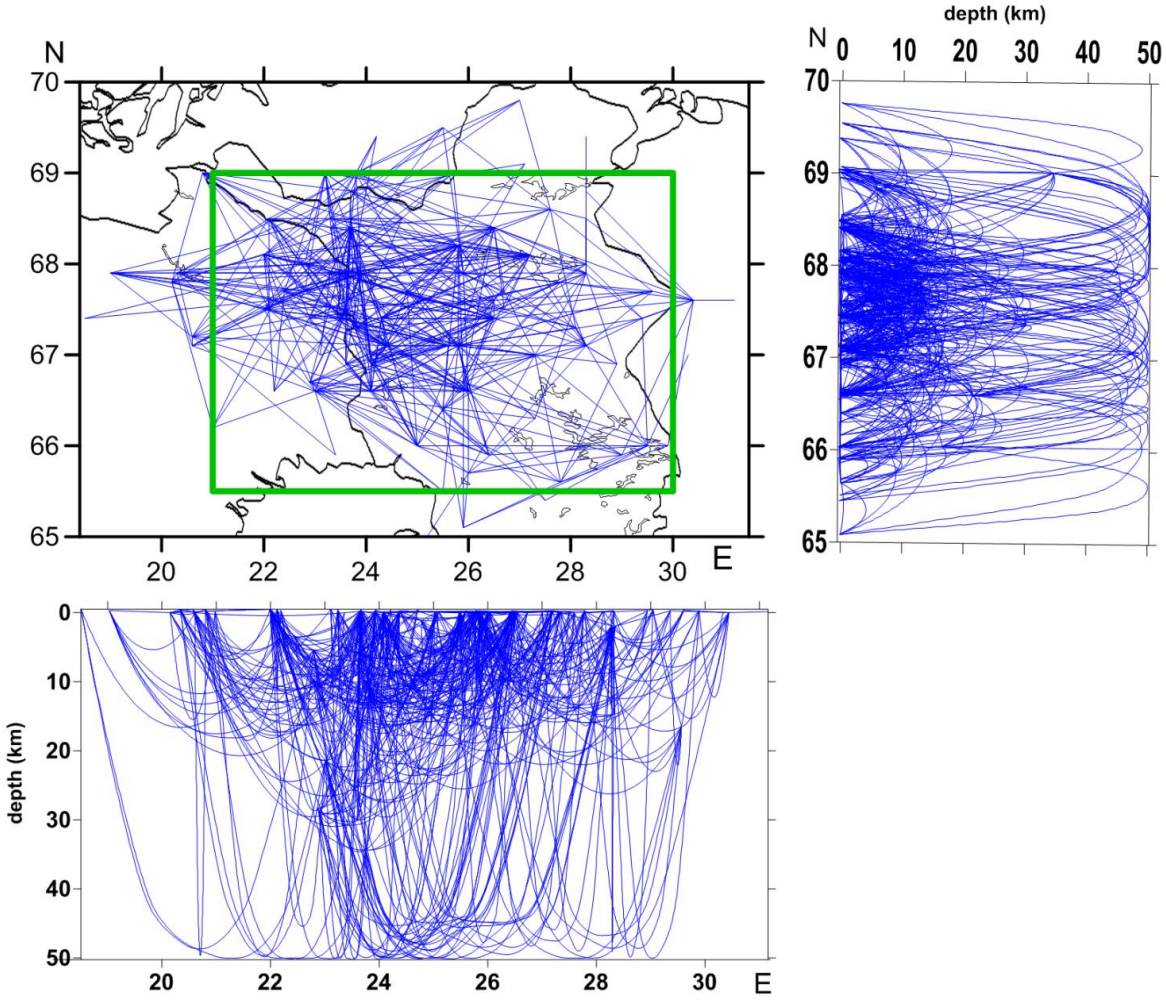

602

603 **Figure 13**

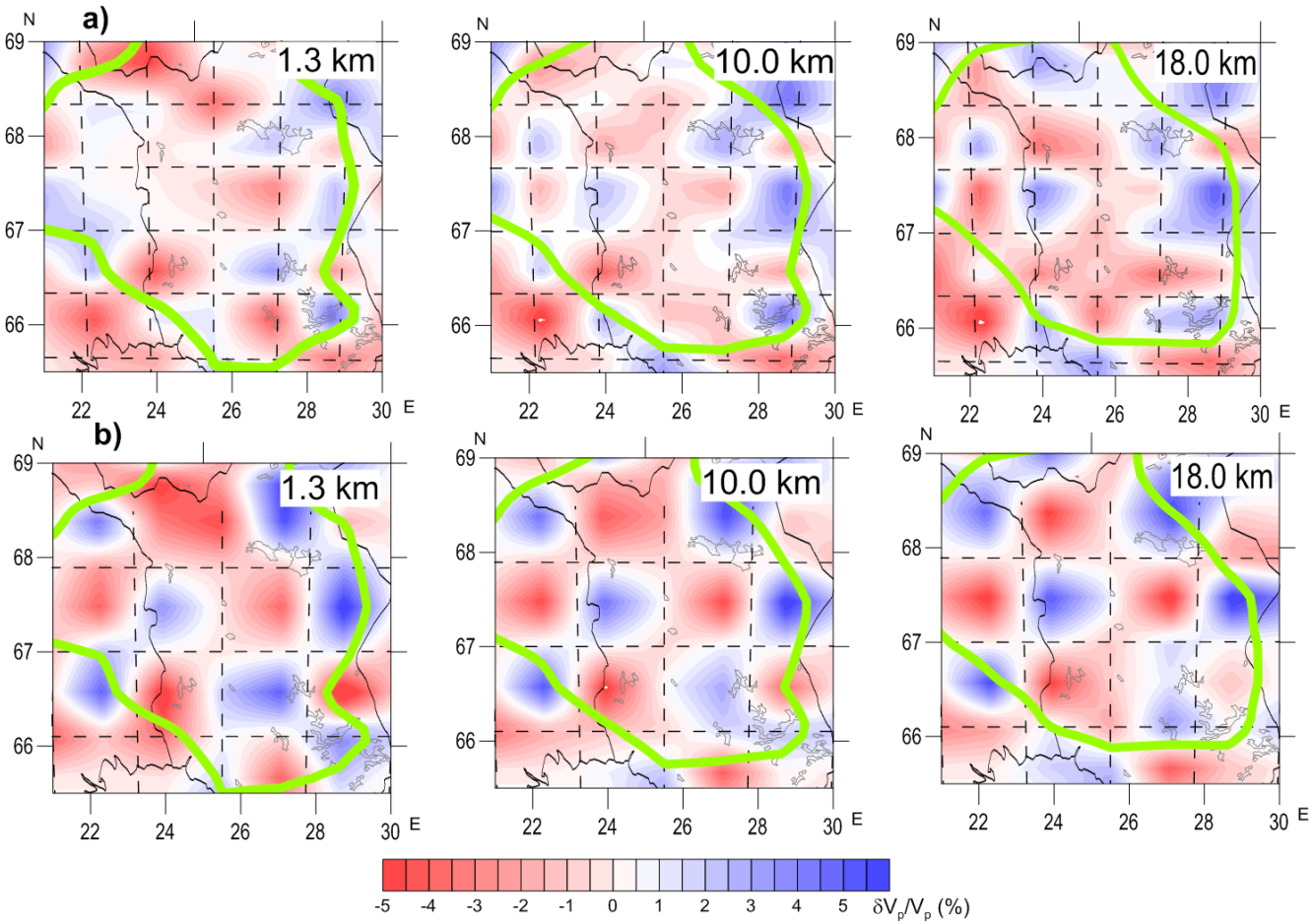
a)
1.3 km
10.0 km
18.0 km
b)
1.3 km
10.0 km
18.0 km
N
E
69
68
67
66
22
24
26
28
30
-5 -4 -3 -2 -1 0 1 2 3 4 5
δVp/Vp (%)

Figure 14

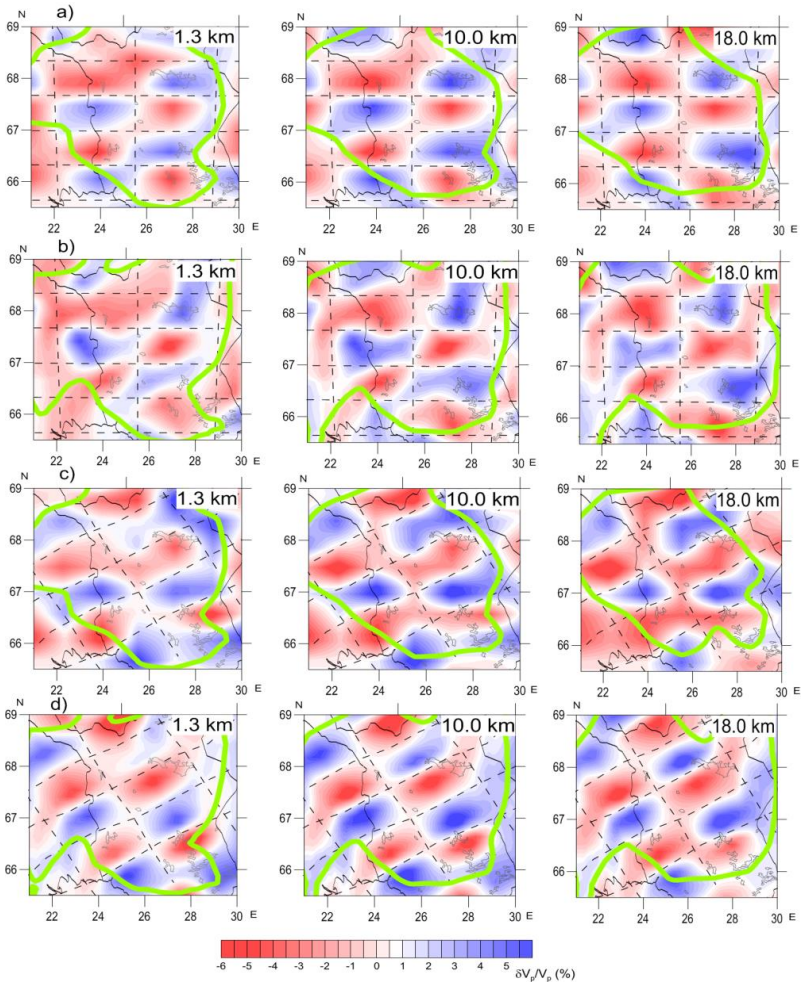

607

608 **Figure 15**

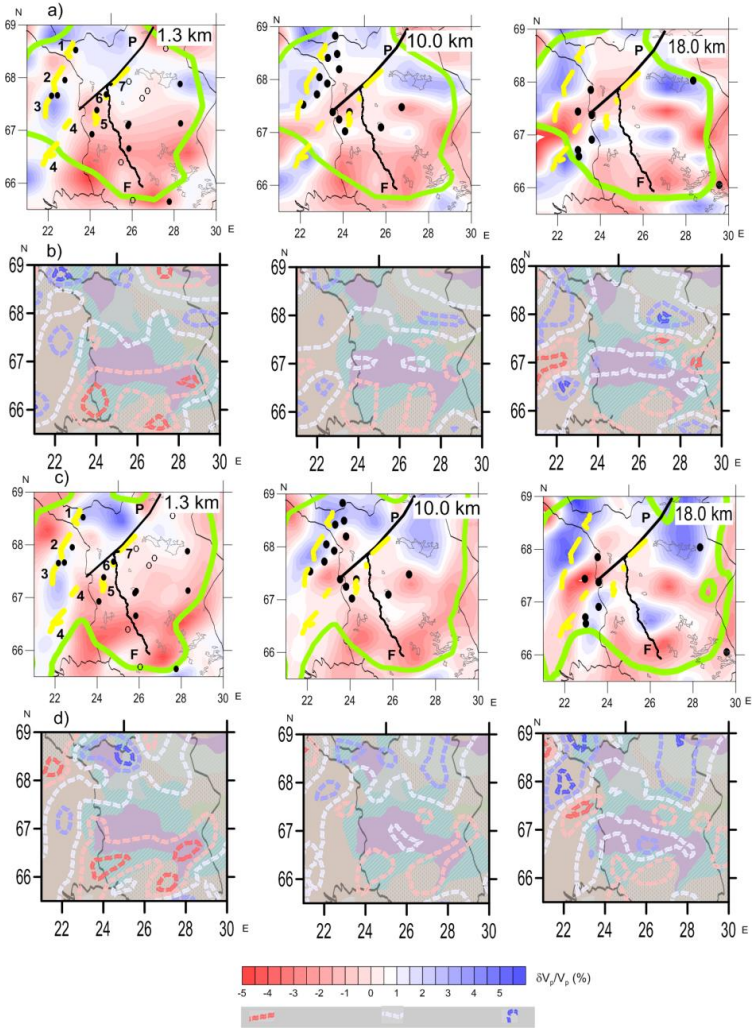

Figure 16

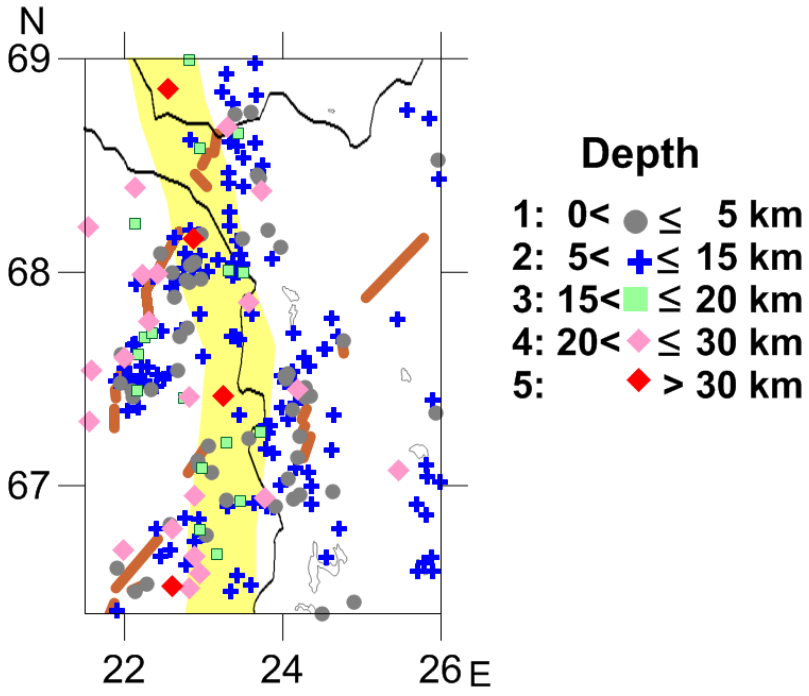

611

612 **Figure 17**

613

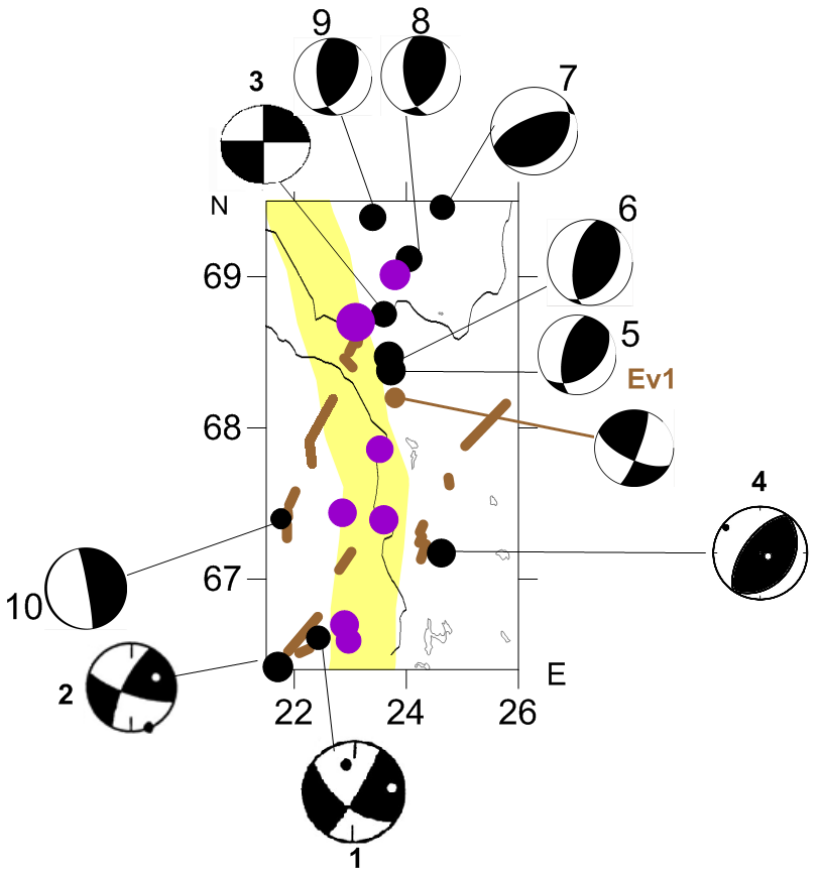

614

615 **Figure 18**